

# Semiflexible polymer rings on topographically and chemically structured surfaces

Petra Gutjahr,<sup>a</sup> Reinhard Lipowsky<sup>a</sup> and Jan Kierfeld<sup>ab</sup>

Received 14th May 2010, Accepted 23rd August 2010

DOI: 10.1039/c0sm00381f

We investigate morphologies of semiflexible polymer rings, such as circular DNA, which are adsorbed onto topographically or chemically structured substrate surfaces. We classify all equilibrium morphologies for two striped surface structures, (i) topographical surface grooves and (ii) chemically structured surface domains. For both types of stripes, we find four equilibrium shapes: a round toroidal and a confined elongated shape as well as two shapes containing bulges. We determine the complete bifurcation diagram of these morphologies as a function of their contour length and the ratio of adhesive strength to bending rigidity. For more complex geometries consisting of several stripes we find a cascade of transitions between elongated shapes. Finally, we compare our findings to ring condensation by attractive interactions.

## 1 Introduction

Bionanotechnology requires the immobilization and controlled manipulation of DNA and other semiflexible polymers. Adsorption is the simplest technique to immobilize single polymers and a first step towards further visualization and manipulation using, *e.g.*, modern scanning probe techniques.<sup>1,2</sup> For manipulation, control over the shape of the adsorbed polymer is needed. In this article, we explore the possibility to achieve such shape control for semiflexible polymer rings using simple striped surface structures, which can be realized by topographical or chemical structuring. Whereas flexible polymers are governed by conformational entropy and typically adsorb in random coil configurations, the morphologies of semiflexible polymers with large persistence lengths are dominated by their bending rigidity, which gives rise to well-defined shapes: An open polymer adsorbs in a straight configuration, whereas a closed polymer ring forms a circular loop. Examples of such semiflexible rings are provided by DNA minicircles,<sup>3</sup> carbon nanotubes<sup>4</sup> filamentous actin,<sup>5</sup> and amyloid fibrils.<sup>6</sup> The shape of such semiflexible rings is of importance for biological issues such as the accessibility in transcription of viral genomes or plasmids or their transport properties.

In the absence of thermal fluctuations or external forces closed semiflexible rings assume a well-defined circular shape. It has been shown that thermal fluctuations lead to interesting effects such as a gradual crossover from oblate spherically symmetric ring shapes at low temperatures or high stiffness to prolate shapes for increasingly flexible rings with a maximal asphericity at intermediate stiffnesses.<sup>7</sup> Semiflexible rings may also be viewed as one-dimensional analogues of two-dimensional vesicles, for which thermal fluctuations gives rise to shape asphericity as well.<sup>8</sup> In this article, we focus on the influence of external forces

or potentials, which tend to confine the semiflexible ring. This issue is of general importance not only to control the shape of semiflexible polymers for further manipulation but also to understand how semiflexible polymers or elastic sheets can be packaged and which forces or potentials are necessary to achieve a given packaging configuration.

In this article, we present a quantitative analysis of shapes of a strongly adsorbed semiflexible polymer ring in the presence of an additional substrate structure, which can be either a topographical surface groove with rectangular cross section, see Fig. 1(a), or a striped domain of increased adhesion energy, see Fig. 1(b). Topographical surface steps have been employed in recent manipulation experiments on semiflexible polymer rings.<sup>9</sup> Adsorption of DNA on grooved, periodically structured substrates has also been investigated in ref. 10,11. Both striped structures introduce a laterally modulated adhesion potential, which attracts the ring to the stripe. We find that, for persistence lengths larger than the stripe width, the competition between its bending rigidity and the attraction to the striped domain allows a controlled switching between four distinct stable morphologies, see Fig. 1. Apart from a weakly bound almost circular shape and a strongly bound elongated shape, bulged intermediate shapes become stable for large contour lengths. We determine the full bifurcation diagrams for semiflexible ring shapes both analytically and numerically. This analysis can be used to (i) control the ring shape and (ii) analyze material properties of the substrate or the semiflexible polymer ring experimentally. Flexible polymer rings, on the other hand, exhibit random coil configurations and do not undergo such morphological transitions. Finally, we generalize our findings to semiflexible polymer rings on a *periodic* stripe pattern, which serves as a model for the interaction between a polymer and the atomic lattice structure of substrate surface.

The condensation of semiflexible polymers such as DNA<sup>12–15</sup> or actin filaments<sup>5,16</sup> is a closely related transition phenomenon that is caused by the competition between attractive interactions and bending energy. In poor solvent, in the presence of condensing agents or depletion forces, polymer-polymer contacts

<sup>a</sup>Max Planck Institute of Colloids and Interfaces, Science Park Golm, 14424 Potsdam, Germany

<sup>b</sup>Physics Department, TU Dortmund University, 44221 Dortmund, Germany

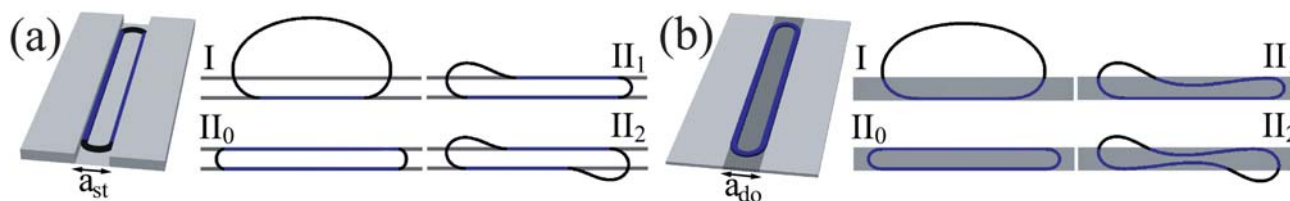


**Fig. 1** Adsorbed polymer on a striped surface containing (a) a rectangular topographical surface groove of width  $a_{st}$  and (b) a chemically structured surface domain of width  $a_{do}$ . Both in (a) and (b), the first perspective drawings illustrate the system geometry whereas the remaining four subfigures represent top views of all four stable ring morphologies I, II<sub>1</sub>, II<sub>0</sub>, and II<sub>2</sub> as obtained by energy minimization for contour lengths  $L/a_{st} = 20$  and  $L/a_{do} = 20$ ; the perspective drawings correspond to the elongated shape II<sub>0</sub>.

become favorable, but the bending rigidity of a semiflexible polymer inhibits its collapse towards a tightly packed globular structure, which is common for flexible polymers. As a result, semiflexible polymers form toroidal bundles<sup>5,13,16</sup> via a cascade of metastable racquet states.<sup>14</sup> At the end of the article, we compare our findings for morphological transitions on structured substrates to the condensation of a semiflexible ring by attractive polymer–polymer interactions.

## 2 Topographical surface groove

### 2.1 Model

We consider a semiflexible polymer ring of fixed contour length  $L$  adsorbed to a planar substrate in the  $xy$ -plane that contains two parallel topographical surface steps at  $x = \pm a_{st}/2$  forming an infinitely long rectangular surface groove of width  $a_{st}$ , see Fig. 1(a). It is further assumed that the overall adhesion is so strong, that the polymer is firmly adsorbed to the substrate surface. We will first focus on polymer morphologies at zero temperature  $T = 0$  and discuss the effect of thermal fluctuations in the end. The polymer gains an additional adsorption energy  $W_{st} < 0$  per polymer length only at the corners of the rectangular surface groove, where it can bind to two adjacent surfaces as shown in Fig. 1(a). The resulting lateral adsorption potential can be described by  $V_{st}(x) = W_{st}$  for  $|x \pm a_{st}/2| < \ell/2$  and  $V_{st}(x) = 0$  otherwise, where  $\ell$  denotes the adhesive range of the surface steps, which is of the order of the polymer diameter and assumed to be small compared to the groove width,  $\ell \ll a_{st}$ .

The bending energy of the polymer is given by

$$E_b = (\kappa/2) \int_0^L ds (\partial_s \theta(s))^2 \quad (1)$$

where  $\kappa$  is the bending rigidity, and the contour is parameterized by the arc length  $s$  ( $0 < s < L$ ) using the tangent angles  $\theta(s)$ . The adhered length  $L_{st}$  is given by the polymer length on the edges at  $x = \pm a_{st}/2$ , and the adhesion energy is

$$E_{ad} = -|W_{st}|L_{st} \quad (2)$$

In the following we often use dimensionless quantities by measuring lengths in units of the groove width, and energies in units of the typical bending energy,

$$\bar{L} \equiv L/a_{st} \text{ and } \bar{E} \equiv E a_{st}/\kappa \quad (3)$$

This leads to  $\bar{E}_{ad} = -|w_{st}|\bar{L}_{st}$  with a *reduced adhesion strength*

$$|w_{st}| \equiv |W_{st}|a_{st}^2/\kappa \quad (4)$$

The polymer configuration is determined by minimizing the total energy  $E_{tot} = E_b + E_{ad}$  under the constraints imposed by ring closure, *i.e.*,  $\int_0^L ds (\cos \theta(s), \sin \theta(s)) = (0, 0)$ . This yields a shape equation for  $\theta(s)$  and an implicit equation for the Lagrange multiplier associated with the ring closure constraint. Solving these equations, the polymer shape and the resulting energies can be calculated analytically.

We assume the surface step height to be comparable to the polymer diameter and neglect small energy corrections arising if the polymer crosses the surface steps. For large step heights and large bending rigidity  $\kappa$  these corrections become important, and a polymer crossing two parallel topographical surface steps can even lift from the groove in this limit.<sup>17</sup>

### 2.2 Energy minima for fixed adhered length

For a single value of the adhesion strength  $W_{st}$  we often find several metastable ring shapes apart from the ring shape representing the stable global energy minimum. In order to determine all metastable states of the total energy  $E_{tot} = E_b + E_{ad}$  and discuss bifurcations of these metastable states, we minimize the *constrained* energy  $E_{tot}(L_{st})$ , where we also fix the adhered length  $L_{st}$  and, thus, the adhesion energy. Then, each metastable state represents a local minimum in the energy landscape given by the function  $E_{tot}(L_{st})$ . If a local minimum vanishes, the corresponding metastable state becomes unstable. If the global minimum exchanges between two local minima, we are at a transition point between two morphologies. Maxima in the constrained energy also allow us to discuss possible transition states of these shape transitions.

For a topographical groove all metastable states consist of one or two straight adhered segments at the corners of the groove and with total length  $L_{st}$ , which are connected by one or two curved segments, respectively. The curved segments are bending energy minimizers, *i.e.*, planar Euler elastica. More than two curved segments are unfavorable. We find four possible metastable morphologies: For small  $L_{st}$ , the ring will adhere only to one corner of the groove and adopt the rather round toroidal configuration I, see Fig. 1. For  $L_{st} \geq L/2$ , conformations of the type II, where the ring binds to both corners, will become relevant. These shapes consist of two round segments connecting straight adhered segments. The round segments can have either the form of a round *cap* staying completely inside the groove or

contain *bulges*, which are round segments outside the groove. All shapes adhering to both corners of the groove may be classified by the number of bulges and are referred to as  $\Pi_0$ ,  $\Pi_1$ , and  $\Pi_2$ , accordingly, see Fig. 1.

In order to minimize bending energy, curved segments in shapes of type II will only bulge to one side of the groove. In principle, also curved segments extending bulges to both sides of the groove resulting in a configuration with reflection symmetry with respect to the  $x$ -axis represent a metastable state. As derived in the appendix, the bending energy of an asymmetric one-sided bulge is lower in bending energy for the same adhered length  $L_{st}$  for all possible adhered lengths. Therefore, we neglect this type of bulges in the following and consider only the remaining four relevant metastable shapes I,  $\Pi_0$ ,  $\Pi_1$ , and  $\Pi_2$ .

The curved segments on both sides of a ring in shapes II can exchange length even if the total adhered length  $L_{st}$  is fixed. This results in the transversality condition that the curvatures at the contact points have to be equal in all four contact points of shapes II. Therefore, bulges or caps on both sides of the ring have to have the same size in shapes  $\Pi_0$  and  $\Pi_2$ . In shape  $\Pi_2$  bulges at both ends can be on either side of the groove, therefore two

energetically degenerate shapes  $\Pi_2$  exist for a topographical groove. The shape with both bulges on the same side has reflection symmetry with respect to the  $y$ -axis, the shape with both bulges on opposite sides, which is shown in Fig. 1(a), is antisymmetric with respect to the center of the shape.

For a topographical stripe the energies of the four types of shapes can be obtained by analytical energy minimization. For fixed adhered length  $L_{st}$  the adhesion energy  $\bar{E}_{ad} = -|w_{st}|\bar{L}_{st}$  is a constant contribution to the constrained energy  $E_{tot}(L_{st})$ . Therefore, the analytical calculation starts by calculating the bending energy  $\bar{E}_b(\bar{L}_{st})$  of all four metastable states as a function of the adhered length  $\bar{L}_{st}$ . This bending energy arises from the curved segments of the ring shape, which take the shape of Euler elastica. To calculate these shapes a constraint for ring closure has to be imposed, which is associated with an additional Lagrange multiplier. For the resulting second order Euler Lagrange equations describing the shapes of curved segments can always find one first integral. We can express contour length  $L$ , adhered length  $L_{st}$  and bending energy  $E_b$  parametrically as functions of a single parameter which is related to the integration constant of the shape equations. Using this method, we derive analytical parametric representations of the bending energy landscape  $\bar{E}_b(\bar{L}_{st})$  in terms of this integration constant parameter in the appendix. In Fig. 2(a) we show the main result of this calculation, which is the bending energy landscape  $\bar{E}_b(\bar{L}_{st})$  consisting of four bending energy branches corresponding to the four different morphologies.

Our analytical results are confirmed by numerical energy minimization using the dynamical discretization algorithm of the SURFACE EVOLVER 2.14.<sup>18</sup> In Fig. 2(a), the bending energy landscapes  $\bar{E}_b(\bar{L}_{st})$  of all four morphologies as obtained from the exact analytical energy minimization are shown as solid lines; the results from numerical energy minimization as colored dots and completely agree with the analytical results.

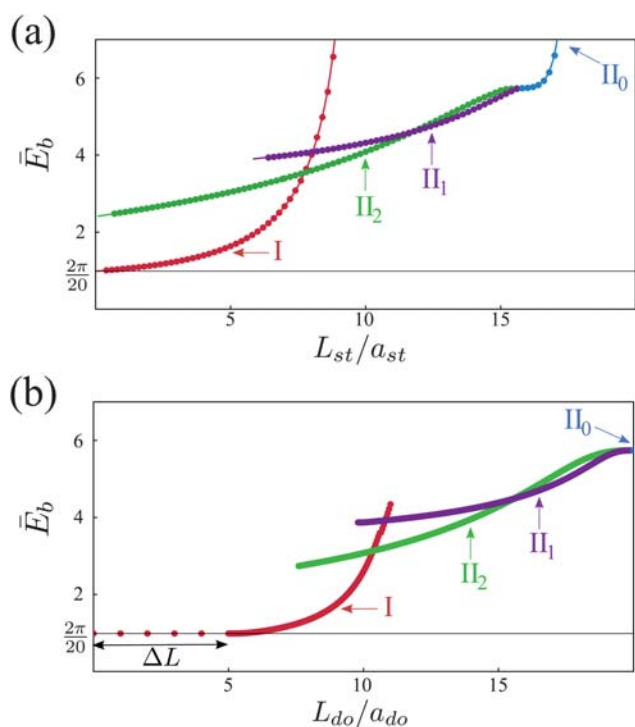


**Fig. 2** (a) The dimensionless bending energy  $\bar{E}_b$  as defined in (3) of the metastable states I (red),  $\Pi_0$  (blue),  $\Pi_1$  (violet), and  $\Pi_2$  (green), as a function of the adhered length  $L_{st}/a_{st}$  for a semiflexible ring of length  $L/a_{st} = 20$  adsorbing on a *topographical surface groove* of width  $a_{st}$ . Solid lines are analytical results, dots represent data from numerical energy minimization. The arrows correspond to the shapes shown in Fig. 1(a). (b) The dimensionless bending energy  $\bar{E}_b$  as defined in (19) of the metastable states as a function of the adhered length  $L_{do}$  (in units of  $a_{do}$ ) for a semiflexible ring of length  $L/a_{do} = 20$  adhering to a *chemically structured stripe* of width  $a_{do}$  from numerical energy minimization. There is an approximately constant shift in the adhered length  $\Delta L$  compared to the results for the topographical stripe in (a). The arrows point to shapes that are displayed in Fig. 1(b).

### 2.3 Unconstrained energy minima

The total energy landscape  $\bar{E}_{tot}(\bar{L}_{st}, |w_{st}|)$  for each morphology is obtained by adding the linearly decreasing adhesion energy  $\bar{E}_{ad} = -|w_{st}|\bar{L}_{st}$  to the corresponding bending energy branch, *i.e.*, by a simple tilt of the bending energy landscape in Fig. 2(a). The local minimum of each branch of the resulting energy landscape  $\bar{E}_{tot}(\bar{L}_{st}, |w_{st}|)$  with respect to the adhered length  $\bar{L}_{st}$  gives the equilibrium total energy of the corresponding morphology I,  $\Pi_0$ ,  $\Pi_1$ , or  $\Pi_2$ . These energy minima depend on the tilt of the bending energy landscape and are, thus, a function of the adhesion strength  $|w_{st}|$ ,

$$\bar{E}_{tot}(|w_{st}|) = \min_{\bar{L}_{st}} (\bar{E}_b(\bar{L}_{st}) - |w_{st}|\bar{L}_{st}) \quad (5)$$

Therefore, the equilibrium total energy  $\bar{E}_{tot}(|w_{st}|)$  is a Legendre transform of the bending energy  $\bar{E}_b(\bar{L}_{st})$  with respect to the adhered length  $\bar{L}_{st}$ . The resulting energy bifurcation diagram Fig. 3(a,b) shows the four branches of the equilibrium total energy  $\bar{E}_{tot}$  for the four local minima as a function of  $|w_{st}|$  for a contour length  $L = 20$ .

If the constraint on the total adhered length is lifted and the total energy minimized with respect to the adhered length, a transversality condition arises at the contact points where the

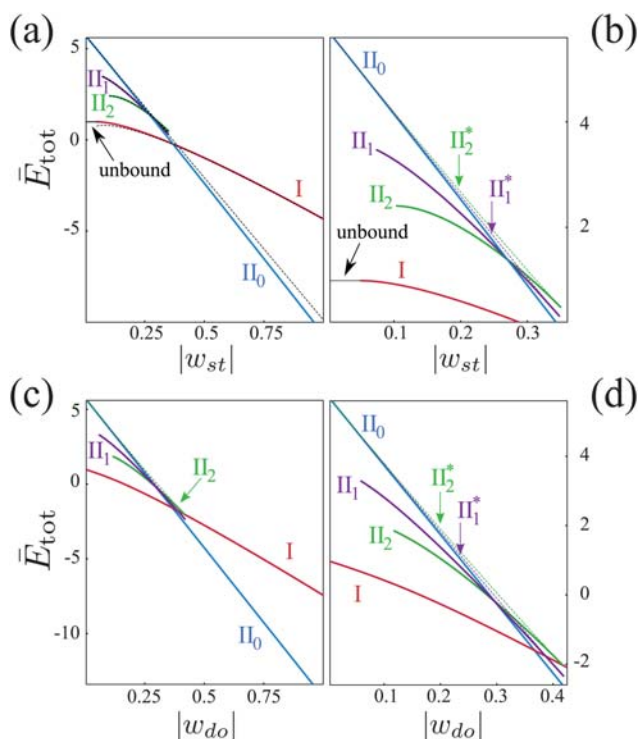


**Fig. 3** (a) The dimensionless total energy  $\bar{E}_{\text{tot}}$  of all metastable states versus the reduced potential  $|w_{st}|$  for a semiflexible ring of contour length  $Ll_{st} = 20$  adsorbing on a *topographical surface groove* of width  $a_{st}$ . The graph shows analytical results for the shapes I,  $\Pi_0$ ,  $\Pi_1$ , and  $\Pi_2$  as red, blue, violet, and green solid lines, respectively. Analytical estimates for these energy curves as derived in the appendix are shown as dashed lines. Lines end where a metastable shape become unstable. (b) A magnification of the upper left corner of (a) including the unstable transition states  $\Pi_1^*$  and  $\Pi_2^*$  as violet and green dashed line, respectively. The analytical estimates are omitted for clarity. (c) Analogous numerical results of the dimensionless total energy  $\bar{E}_{\text{tot}}$  as a function of  $|w_{do}|$  for a semiflexible ring adhered to a *chemically structured stripe* with  $Ll_{do} = 20$  and magnified in (d). The unbound circle is never stable and therefore absent for the chemical domain.

curved segments join the straight segments adhered on the surface steps. According to this transversality condition the curvature at the contact points is given by the inverse contact radius<sup>19,20</sup>

$$1/R_{co} = (2|W_{st}|/\kappa)^{1/2} \quad (6)$$

In the limit of small bending rigidity  $\kappa$  and large adhesion strength  $|W_{st}|$  the contact radius becomes small compared to the groove width,  $R_{co} \ll a_{st}$ , corresponding to  $|w_{st}| \gg 1$  for the reduced adhesion strength (4). In this limit, the ring assumes an effectively kinked shape  $\Pi_0$ , in which caps on both sides of the ring become almost straight and the ring shape resembles a rectangle with sharp kinks, similar to shapes that have been observed in ref. 10,11. Only on length scales smaller than the contact radius  $R_{co}$  these sharp kinks can be resolved as smooth bends.

In the appendix we present exact analytical results for the unconstrained total energy  $\bar{E}_{\text{tot}}(|w_{st}|)$ : using the condition of contact curvature at the end points of all curved segments, we

derive analytical parametric representations of the total energy  $\bar{E}_{\text{tot}}(|w_{st}|)$  in terms of the same integration constant parameter which we used for the bending energy landscapes  $\bar{E}_b(\bar{L}_{st})$ . In the following, we focus on approximate results for the total energy and outline the main features of the bifurcation diagram.

In the bifurcation diagram Fig. 3(a,b), the globally stable ring shape is the shape with the lowest energy  $\bar{E}_{\text{tot}}$  for a given adhesion strength  $|w_{st}|$ . If two branches of local minima in the bifurcation diagrams in Fig. 3 cross or merge, a morphological transition between the corresponding shapes occurs. If the branches cross at a finite angle, this transition is discontinuous with hysteresis effects and jumps in the adhered length  $L_{st}$ , which is given by the negative slope  $L_{st} = -\partial_{|w_{st}|}\bar{E}_{\text{tot}}(|w_{st}|)$  according to (5). As can be seen from the bifurcation diagram Fig. 3(a,b) all shape transition between the four metastable states are *discontinuous*, which gives rise to many metastable shapes and shape hysteresis. A metastable state becomes unstable if the corresponding branch ends. In particular, this happens for the two bulged shapes  $\Pi_1$  and  $\Pi_2$ , which are only metastable for a limited range of adhesion strengths  $|w_{st}|$ .

Apart from discontinuous transitions between the four shapes, shape I undergoes an additional *continuous* unbinding transition from a single surface step, which is also known for vesicles adhering to a surface, where the interplay between adhesion and bending energy leads to an unbinding transition, which is not driven by thermal fluctuations.<sup>19,20</sup> A transversality condition enforces the curvature at the contact point to be  $1/R_{co} = (2|w_{st}|)^{1/2}/a_{st}$ , see eqn (6), such that rings of contour length  $L$  can only bind to the contact line for  $\bar{L} \geq \bar{L}_{ub}$  with

$$\bar{L}_{ub} = \sqrt{2\pi}|w_{st}|^{-1/2} \quad (7)$$

In the energy bifurcation diagrams Fig. 3(a,b) the round configuration I (red line) represents the global energy minimum for small  $|w_{st}|$ , whereas the adhesion energy gain dominates for large  $|w_{st}|$ , and the elongated shape  $\Pi_0$  (blue line) becomes the globally stable conformation. For adhesion strengths  $|w_{st}|\bar{L}^2 \gg 2\pi^2$  corresponding to contour lengths much larger than the contact radius,  $L \gg R_{co}$ , shape I can be approximated by two semicircles of contact radius  $R_{co}$  connected by two straight segments, one of which is adhered to one step edge. This results in  $\bar{E}_1 \approx -|w_{st}|\bar{L}/2 + 3\pi|w_{st}|^{1/2}/\sqrt{2}$  for the total energy. The exact calculation in the appendix gives a total energy

$$\bar{E}_1 \approx -|w_{st}|\bar{L}/2 + 4\sqrt{2}|w_{st}|^{1/2} \quad (8)$$

for  $|w_{st}|\bar{L}^2 \gg 2\pi^2$ , which only differs in one prefactor.

Shape  $\Pi_0$  can be approximated by two semicircular caps of diameter  $a_{st}$ , which contribute a bending energy  $\bar{E}_b \approx 2\pi$ , connected by two straight adhered segments of length  $L_{st} = L - \pi a_{st}$ . This gives a total energy

$$\bar{E}_{\Pi_0} \approx 2\pi - |w_{st}|(\bar{L} - \pi) \quad (9)$$

for the total energy of shape  $\Pi_0$ . Note that shape  $\Pi_0$  can only be realized for rings with  $\bar{L} > \pi$  such that the ring can touch both step edges if it assumes a circular form. For intermediate adhesion strengths  $|w_{st}| \approx 2$ , this result agrees with the exact calculation. For weak adhesion strengths  $|w_{st}| \ll 1$ , the exact calculation in the appendix gives a total energy



$$\bar{E}_{\text{II}_0} \approx 5.74 - |w_{st}|(\bar{L} - 4.38) - 1.31|w_{st}|^{3/2} \quad (10)$$

which differs only slightly in the numerical prefactors.

The energy branches corresponding to shapes I and  $\text{II}_0$  cross resulting in a *discontinuous* morphological transition between these two shapes with a jump in the adhered length  $L_{st}$ . In the vicinity of this transition also the shapes  $\text{II}_1$  and  $\text{II}_2$  become stable or metastable, which develop from the elongated shape  $\text{II}_0$  by the formation of one and two *bulges*, respectively. We can approximate the bulge by a semicircle with diameter  $d_{\text{bul}} > a_{st}$  and a weakly bent desorbed segments connecting this semicircle to the stripe edge, and determine the diameter  $d_{\text{bul}}$  and the length of the desorbed segment by optimizing the sum of bending energy gain and adhesion energy cost. For small  $|w_{st}|$ , this approximation gives an optimal bulge diameter  $d_{\text{bul}} \sim a_{st}|w_{st}|^{-1/2} \sim R_{co}$ , which is proportional to the contact radius, and a total energy cost  $\Delta\bar{E}_{\text{bul}} \approx -\pi + 7.46|w_{st}|^{1/2} - 2.92|w_{st}|$  for creating one bulge starting from the confined shape  $\text{II}_0$ , which is independent of  $L$ .

The exact calculation in the appendix gives

$$\Delta\bar{E}_{\text{bul}} \approx -2.87 + 7.50|w_{st}|^{1/2} - 3.72|w_{st}| + 0.30|w_{st}|^{3/2} \quad (11)$$

for  $|w_{st}| \ll 1$ , which only slightly differs in the numerical prefactors. The resulting energies of both bulged shapes  $\text{II}_m$  are exactly given by  $\bar{E}_{\text{II}_m} = \bar{E}_{\text{II}_0} + m\Delta\bar{E}_{\text{bul}}$  ( $m = 0, 1, 2$ ) as shown in the appendix. The bulges are thus localized and non-interacting excitations of shape  $\text{II}_0$ . The energy branches of shapes  $\text{II}_m$  thus all intersect in a single point in the bifurcation diagram Fig. 3(a,b), which is determined by the condition  $\Delta\bar{E}_{\text{bul}} = 0$ . For  $\Delta\bar{E}_{\text{bul}} < 0$ , shape  $\text{II}_2$  with two bulges is energetically favorable, whereas for  $\Delta\bar{E}_{\text{bul}} > 0$ , shape  $\text{II}_0$  without bulges is energetically favorable. Therefore, shape  $\text{II}_1$  with one bulge is *never* globally stable and, thus, there are only bulging transitions from shape  $\text{II}_0$  directly into shape  $\text{II}_2$ . Moreover, the shape transitions from shape  $\text{II}_2$  into shapes  $\text{II}_0$  or I are *discontinuous*.

We also show in the appendix analytically that bulges are only metastable for a limited range of adhesion strengths  $w_{\text{min}}(\bar{L}) < |w_{st}| < w_{\text{max}}$ . For the upper stability limit we find the universal value  $w_{\text{max}} \approx 0.35$ , which holds both for shape  $\text{II}_1$  with a single bulge and shape  $\text{II}_2$  with two bulges. For  $|w_{st}| > w_{\text{max}}$ , bulges become unstable with respect shrinking to zero size, and the bulged shapes become unstable with respect to a spontaneous transition into shape  $\text{II}_0$ . The lower stability limit  $w_{\text{min}}(\bar{L})$  depends on the contour length of the ring and slightly differs for shapes  $\text{II}_1$  and  $\text{II}_2$ . For  $|w_{st}| < w_{\text{min}}(\bar{L})$ , the bulges become so large that the adhered length on one or both of the surface steps shrinks to zero length, and the bulged shapes become unstable with respect to a spontaneous transition into shape I. For  $\bar{L} = 20$  as in the bifurcation diagram Fig. 3(a,b), we find  $w_{\text{min}} \approx 0.10$  for shape  $\text{II}_2$  and  $w_{\text{min}} \approx 0.07$  for shape  $\text{II}_1$ .

The energies of the four metastable shapes can be probed in an ensemble of adsorbed polymer rings of equal length  $L$ . The relative frequency of each shape is proportional to the Boltzmann weight associated with its energy.

## 2.4 Morphology diagram

The full morphology diagrams Fig. 4(a,b) shows how the stability of the four shapes I,  $\text{II}_0$ ,  $\text{II}_1$  and  $\text{II}_2$  is controlled by the

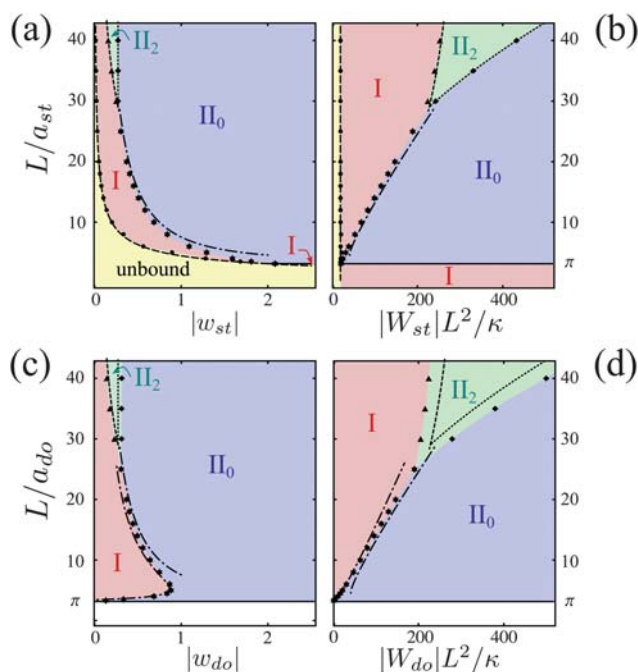


**Fig. 4** Morphology diagram for a ring of length  $L$  adhering to a *topographical surface groove* of width  $a_{st}$  as a function of (a) the contour length  $L/a_{st}$  and the reduced potential strength  $|w_{st}|$  as defined in (4) and (b)  $L/a_{st}$  and  $|W_{st}|L^2/\kappa = |w_{st}|L^2/a_{st}^2$ . For a *chemical domain* of width  $a_{do}$ , the morphology diagram is shown as a function of (c)  $L/a_{do}$  and  $|w_{do}|$  as defined in (17) or (d)  $L/a_{do}$  and  $|W_{do}|L^2/\kappa$ . The parameter choice in (b) and (d) is advantageous if the structure width  $a_{st}$  and  $a_{do}$  is varied, while the other system parameters are kept constant. Morphological transitions as obtained from analytical energy minimization in (a) and (b) and from numerical energy minimization in (c) and (d) are represented by stars, triangles, diamonds and dots. The results (12), (13), and (15) for these transitions are indicated as dot-dashed, dotted and dashed lines, respectively. In (a) and (b) the dashed line marks the unbinding transition, whereas in (c) and (d) the dashed line marks the reentrant transition for small rings.

parameters  $|W_{st}|$ ,  $L$ , and  $a_{st}$ . Phase boundaries from numerical minimization are denoted by symbols. The dashed line corresponds to the continuous unbinding transition (7) and agrees with the numerical results. The main feature of the morphology diagrams is the discontinuous transition between morphologies I and  $\text{II}_0$ , (stars). Going through this transition with increasing  $|w_{st}|$ , the ring goes from the round toroidal configuration I into the confined elongated configuration  $\text{II}_0$ . The location of this transition can be derived from the condition  $\bar{E}_I = \bar{E}_{\text{II}_0}$ . Using the estimates (8) and (9) given above we find a transition line

$$\bar{L}_{\text{I-II}_0} \approx 2\pi - 8\sqrt{2}|w_{st}|^{-1/2} + 4\pi|w_{st}|^{-1} \quad (12)$$

valid for  $|w_{st}| \lesssim 2$  and shown as dash-dotted line in Fig. 4(a,b).

This transition line terminates at  $\bar{L} = \pi$  and  $|w_{st}| = 2$  where it intersects the unbinding transition line. For strong adhesion with  $|w_{st}| > 2$  a short ring first adheres to one corner of the groove for  $\bar{L} = \bar{L}_{ub} < \pi$  in a round shape I, which, however, lies completely *inside* the groove. Only for  $\bar{L} > \pi$ , the ring touches the opposite corner of the groove and immediately assumes the elongated shape  $\text{II}_0$  because shape I is unstable in this regime, see Fig. 4(a,b).

At the transition line between configurations  $\text{II}_0$  and  $\text{II}_2$  (diamonds), which occurs for large  $\bar{L}$ , it becomes energetically favorable to form bulges on top of the confined shape  $\text{II}_0$ , *i.e.*, the energy difference  $\Delta\bar{E}_{\text{bul}}$  becomes negative. Also this bulging transition is discontinuous. Because both the caps of shape  $\text{II}_0$  and the bulges of shape  $\text{II}_2$  have a finite length, the bulge energy  $\Delta\bar{E}_{\text{bul}}$  only depends on  $|w_{st}|$  and is independent of the contour length  $L$ . Therefore the transition line between configurations  $\text{II}_0$  and  $\text{II}_2$  is also independent of  $L$  and, thus, vertical in Fig. 4(a). The exact location of the bulging transition line can be found numerically by equating the exact parametric representations of the total energies  $\bar{E}_{\text{tot,II}_0}$  and  $\bar{E}_{\text{tot,II}_2}$  and the corresponding parametric representations of  $|w_{st}|$  given in the appendix, which gives

$$|w_{\text{II}_0-\text{II}_2}| \approx 0.27 \quad (13)$$

and is shown as dotted line in Fig. 4(a,b). Stable bulges form if the energy of a single bulge is negative for  $|w_{st}| < |w_{\text{II}_0-\text{II}_2}|$ . Because bulges are non-interacting, it is always energetically favorable to create two bulges such that shape  $\text{II}_1$  is only metastable and absent in the morphology diagrams, as already mentioned above.

The bulged configuration  $\text{II}_2$  can become stable only above a *triple point*, where the three shapes I,  $\text{II}_0$ , and  $\text{II}_2$  coexist. The exact location of the triple point can be found numerically by equating the parametric representations of the total energies  $\bar{E}_{\text{tot,I}}$ ,  $\bar{E}_{\text{tot,II}_0}$ , and  $\bar{E}_{\text{tot,II}_2}$  and the corresponding parametric representations of  $|w_{st}|$  given in the appendix. This gives

$$|w_{\text{tri}}| = |w_{\text{II}_0-\text{II}_2}| \text{ and } \bar{L}_{\text{tri}} \approx 29.2 \quad (14)$$

Only sufficiently large rings  $\bar{L} > \bar{L}_{\text{tri}}$  can undergo a bulging transition. For shorter rings bulges are unstable and the ring directly assumes the round shape I.

For short rings  $\bar{L} < \bar{L}_{\text{tri}}$ , we can obtain the transition line between shapes  $\text{II}_2$  and I (triangles) using the condition  $\bar{E}_I = \bar{E}_{\text{II}_2} = \bar{E}_{\text{II}_0} + 2\bar{E}_{\text{bul}}$ . Using the estimates (8), (10) and (11) given above we find a transition line

$$\bar{L}_{\text{I-II}_2} \approx -6.13 + 18.68|w_{st}|^{-1/2} - 1.44|w_{st}|^{1/2} \quad (15)$$

for  $|w_{st}| \ll 1$  shown as dashed line in Fig. 4(a,b).

The results (13) and (14) for the bulging transition and the triple point are exact and the approximate formulas (12) for the transition between shapes I and  $\text{II}_0$  and (15) for the transition between shapes I and  $\text{II}_2$  are in good agreement with the numerical results and exact analytical results derived in the appendix as can be seen in the morphology diagrams in Fig. 4(a,b).

The transition lines depend on the control parameters of the system, hence, measurements of these transition lines can be used to determine material parameters, such as  $|W_{st}|$  or  $\kappa$ , experimentally. As opposed to other experimental methods to determine the bending rigidity no *external* forces, *e.g.* via an AFM tip, have to be applied to the polymer, but the substrate pattern itself exerts forces on the ring. In the morphology diagram Fig. 4(a) we use the reduced contour length  $\bar{L}$  and the reduced adhesion strength  $|w_{st}|$  as control parameters. In an experiment, the transition lines in the morphological diagram Fig. 4(a) are crossed in

horizontal direction by changing the adhesion strength  $|W_{st}|$  of the substrate, which could be achieved by changing the substrate chemistry or surface charge. On the other hand, one could use rings of different length on the same substrate and thereby observe ring morphologies along a vertical line in Fig. 4(a). The last and maybe simplest experiment is to fabricate substrates with several grooves of different width  $a_{st}$ . In this case, one would change the ratio of the involved length scales  $\bar{L}$  and the reduced adhesion strength  $|w_{st}|$  at the same time. Therefore, it is much more convenient to characterize the system by  $\bar{L}$  and the control parameter  $|W_{st}|L^2/\kappa = |w_{st}|L^2$  as in the morphology diagram Fig. 4(b). Changing the groove width and thus  $\bar{L} = L/a_{st}$  corresponds to a vertical trajectory in this diagram.

All shape transitions between shapes I,  $\text{II}_0$ , and  $\text{II}_2$  are discontinuous. Therefore shapes remain metastable over a considerable parameter range, which gives rise to strong shape hysteresis along if any transition line is crossed in the morphology diagrams Fig. 4(a,b). For a shape transition from a metastable state to another metastable or stable state a transition state corresponding to a saddle in the energy landscape has to be crossed. For some of the transitions this transition state should also belong to one of the four classes of shapes I,  $\text{II}_0$ ,  $\text{II}_1$ , or  $\text{II}_2$ . For example, state  $\text{II}_0$  remains metastable down to adhesion strengths  $|w_{st}| = 0$ . The transition states for transitions from  $\text{II}_0$  into states  $\text{II}_i$  should also be bulged states. Starting from shape  $\text{II}_0$ , bulged states form by crossing the maxima  $\text{II}_1^*$  or  $\text{II}_2^*$  containing *small* unstable bulges. The shape  $\text{II}_2^*$  corresponds to a shape with two identical small bulges which are unstable with respect to shrinking to zero size to a shape  $\text{II}_0$  or to expanding to its equilibrium size in state  $\text{II}_2$ . Likewise, the shape  $\text{II}_1^*$  contains a single small bulge which is unstable with respect shrinking to zero size to a shape  $\text{II}_0$  or to expanding to its equilibrium size in state  $\text{II}_1$ . There will be an additional transition state between states  $\text{II}_1$  to  $\text{II}_2$  containing one small and one large bulge, where the small bulge is unstable with respect to shrinking to zero size to shape  $\text{II}_1$  or expanding to equilibrium size to state  $\text{II}_2$ .

State I remains metastable for large adhesion strengths until the round unbound segment touches the opposite corner of the groove in its midpoint, which happens for  $|w_{st}| \approx 14.2$ . For transitions between states I and  $\text{II}_i$ , where the round unbound segment attaches to the opposite corner of the groove, the transition state will presumably not fall into one of the four classes of stable states. For large  $|w_{st}|$  state I will attach to the second corner of the groove by deforming asymmetrically.

## 2.5 Thermal fluctuations

The transition states represent local maxima in the energy landscape. Energy differences between the transition state and the corresponding minima give energy barriers for shape transformations. Thermal fluctuations allow the polymer ring to overcome these energy barriers if  $\Delta E < T$  ( $k_B \equiv 1$ ), which is equivalent to  $\Delta\bar{E} < 2a_{st}/L_p$  for a semiflexible polymer with a persistence length  $L_p = 2\kappa/T$ . Therefore, the influence of thermal fluctuations crucially depends on the ratio  $L_p/a_{st}$ : Our results apply for persistence lengths much larger than the stripe width,  $L_p/a_{st} \gg 1$ , where energy barriers are relevant. Then all four (meta-)stable ring shapes are observable, and their morphological transitions exhibit a pronounced hysteretic

behaviour. For flexible polymers with  $L_p/a_{st} \ll 1$ , on the other hand, thermal fluctuations allow the polymer to change orientation within the groove such that the four morphologies can no longer be clearly distinguished.

A single surface step represents a potential well of depth  $|W_{st}|$  and width  $\ell$  comparable to the polymer diameter. Strong thermal fluctuations can give rise to a thermal unbinding transition from a single step if the potential strength is smaller than a critical value,  $|W_{st}| < |W_{st,c}| = cT/L_p^{1/3}\ell^{2/3}$  with a prefactor  $c$  of order unity,<sup>21,22</sup> which is equivalent to a critical value

$$|w_{st}| < |w_{st,c}| = 2ca_{st}^2/L_p^{4/3}\ell^{2/3} \quad (16)$$

for the reduced adhesion strength. For  $|W_{st}| < |W_{st,c}|$  binding to surface steps is prevented by thermal fluctuations and no morphological transitions can be observed. Before but close to thermal unbinding,  $|W_{st}| \lesssim |W_{st,c}|$ , a reduced free binding energy per length  $f_{st} \sim W_{st} - W_{st,c}$ , which includes also entropic contribution should be used instead of the bare adhesion strength  $W_{st}$ .<sup>22</sup>

All morphological transitions derived above in the absence of thermal fluctuations happen for reduced adhesion strength of order unity. Therefore, these results apply also in the presence of thermal fluctuations under the condition  $|w_{st,c}| \ll 1$ , such that thermal unbinding does not interfere with the morphological transitions. The condition  $|w_{st,c}| \ll 1$  is equivalent to sufficiently small polymer diameters  $\ell/a_{st} \ll a_{st}^2/L_p^2$  or sufficiently wide grooves  $a_{st} \gg \ell^{1/3}L_p^{2/3}$ . For typical polymer diameters in the nanometer regime and persistence lengths in the range of 50 nm (DNA) up to 10  $\mu\text{m}$  (filamentous actin), this condition is fulfilled for groove widths  $a_{st} \gg 10$  nm for DNA and  $a_{st} \gg 500$  nm for filamentous actin, respectively. Even if morphological transitions are not modified, thermal unbinding can preempt the bending energy induced ring unbinding transition with  $\bar{L}_{ub} \propto |w_{st}|^{-1/2}$ , see eqn (7), but only for large ring contour lengths  $\bar{L} > |w_{st,c}|^{-1/2}$ .

### 3 Chemically structured striped surface domain

The chemically structured stripe of width  $a_{do}$  is modeled by an additional adhesion energy gain  $W_{do} < 0$  per polymer length for  $|x| \leq a_{do}/2$ , which leads to a generic square well adsorption potential with  $V_{do}(x) = 0$  for  $|x| > a_{do}/2$  and  $V(x) = W_{do}$  for  $|x| \leq a_{do}/2$ . The adhered length  $L_{do}$  is given by the polymer length within the stripe  $|x| \leq a_{do}/2$ , and the adhesion energy is  $E_{ad} = -|W_{do}|L_{do}$ .

The analytical energy minimization becomes involved for the chemical surface domain because adhered segments are no longer perfectly straight as for the topographical groove. Therefore, we performed the energy minimization numerically using the SURFACE EVOLVER. We find the same four types of morphologies I,  $\text{II}_0$ ,  $\text{II}_1$ , and  $\text{II}_2$  as for the topographical groove, see Fig. 1(b). Also for the chemically structured stripe, there are two possible shapes  $\text{II}_2$ , one with bulges on the same side and one with bulges on opposite sides. Both configurations have very similar energies but are no longer strictly degenerate as for the topographical groove: The antisymmetric shape with bulges on opposite sides as shown in Fig. 1(b) has a slightly lower energy for the chemically structured stripe.

Remarkably, ring shapes minimizing the bending energy are almost identical as compared to a topographical groove of the same width  $a_{st} = a_{do}$ , see Fig. 1. Furthermore, the bending energies of constrained equilibrium shapes agree to a good approximation if the adhered length  $L_{do} \approx L_{st} + \Delta L_{ad}$  is shifted by a constant amount  $\Delta L_{ad}$ . In contrast to the groove, the stripe domain is also adhesive between its boundaries for  $|x| < a_{do}/2$  such that the same ring shape has a larger adhered length. As a result of this shift, the bifurcation diagram for the total energies of all local extrema as a function of the reduced adhesion strength

$$|w_{do}| \equiv |W_{do}|a_{do}^2/k \quad (17)$$

resembles the corresponding diagram Fig. 3 for a surface groove.

For shape  $\text{II}_0$  we can show this quantitatively because the total energy of shape  $\text{II}_0$  can be exactly calculated for the chemical domain,

$$\bar{E}_{\text{II}_0} = 5.74 - |w_{do}|\bar{L} \quad (18)$$

where we used the reduced length and reduced energies

$$\bar{L} \equiv L/a_{do} \text{ and } \bar{E} \equiv E a_{do}/k \quad (19)$$

analogously to the topographical groove. As compared to the result (10) for the topographical groove we notice the agreement in the limit of small adhesion strengths with a constant shift  $\Delta\bar{L}_{ad} = 4.38$  of the adhered length. For the shape  $\text{II}_0$  this shift corresponds exactly to the length of the curved caps in the limit of weak adhesion as discussed in the appendix.

As a result of this approximate mapping of shapes and energies between the two types of adhesive stripes, the morphology diagrams in the plane spanned by the reduced potential strength  $|w_{do}|$  and  $\bar{L}$ , as shown in Fig. 4(c,d), look very similar for the chemical stripe and the topographical surface groove. In particular, our results (12) for the transition between shapes I and  $\text{II}_0$  (dash-dotted line in Fig. 4(c,d)), (13) for the appearance of bulged states (dotted line), and (15) for the transition between shapes I and  $\text{II}_2$  (dashed line) remain valid and agree well with the numerical results (stars, diamonds, and triangles, respectively).

However, the unbinding transition of shape I is absent for the chemical stripe domain: it is always energetically favorable for the ring to adhere to the striped domain. Furthermore, the two phase diagrams differ in the behavior of small rings. Small rings can fully bind to the chemical stripe without deformation and shapes I and  $\text{II}_0$  become equivalent, which leads to the re-entrance of shape  $\text{II}_0$  close to  $\bar{L} = \pi$ . We estimate the location of this re-entrant transition can be approximating small rings in shape I by a circle. The adhered length of such a circle is  $\bar{L}_{do} = \bar{L}\arccos(1 - 2\pi/\bar{L})/\pi$  so that the total energy is

$$\bar{E}_1 \approx 2\pi^2/\bar{L} - |w_{do}|\bar{L}_{do} \quad (20)$$

Equating this energy with the total energy (18) of shape  $\text{II}_0$  we find

$$|w_{\text{I-II}_0}| \approx \frac{\pi(5.74\bar{L} - 2\pi^2)}{\bar{L}^2\arccos(2\pi/\bar{L} - 1)} \quad (21)$$



for  $\bar{L} > 3.44$ . This result is also shown as dash-dotted line in Fig. 4(c,d) and gives remarkable agreement with the exact numerical results (stars) also for lengths up to the triple point. Because of the re-entrance the elongated shape  $\Pi_0$  is the stable state for adhesion strengths  $|w_{do}| > 0.86$ .

#### 4 Periodic stripe structures

An important generalization of our system, which can serve as a model for the atomic lattice structure of substrates, is a *periodic stripe pattern*. Specifically, we consider an array of equidistant parallel topographical surface steps located at  $x = ia_{st}$  as they occur, e.g. on vicinal surfaces, see Fig. 5. For surface step heights smaller or comparable to the polymer diameter we can neglect small energy corrections arising if the polymer crosses the surface steps. Then upward and downward steps have the same effect on ring shapes and the two surface step patterns shown in Fig. 5 give rise to approximately identical metastable ring morphologies with almost identical energies.

Such surface structures drastically increase the number of metastable polymer shapes. Before presenting general results for the full periodic pattern, we start by adding a single parallel surface step to the groove shown in Fig. 1(a) at distance  $a_{st}$ . The resulting metastable ring morphologies can be classified into conformations that adhere to one (I), two (II) or three (III) edges plus the unbound circular shape. Clearly, the shapes I are the same as for the single stripe, as the remaining steps (up to small corrections) do not contribute to the energy and also the unbinding transition applies without modifications to the three-step-geometry.

Moreover, if the ring binds to two edges, it should attain shapes that correspond to the morphologies  $\Pi_0$  and  $\Pi_2$  we found before but now the ring can adhere either to two neighboring steps (at a distance  $a_{st}$ ) or to the two outer steps (at a distance  $2a_{st}$ ). Formally, we will distinguish these two cases *via* a superscript that indicates the distance between the relevant edges in units of  $a_{st}$ , i.e.,  $\Pi_0^1$ ,  $\Pi_0^2$  etc. By analyzing the corresponding energy estimates  $E_{tot}(|w_{st}|)$  one finds, that shape  $\Pi_0^2$  is always energetically favorable compared to shape  $\Pi_0^1$ . Furthermore, shape  $\Pi_0^2$  becomes only stable for very large rings, i.e.  $L/2a_{st} > \bar{L}_{tri} \approx 29.2$ . Therefore, shapes with bulges can be neglected altogether to a good approximation.

Now we address the full periodic stripe pattern. Neglecting the formation of bulges the possible stable states are shape I and

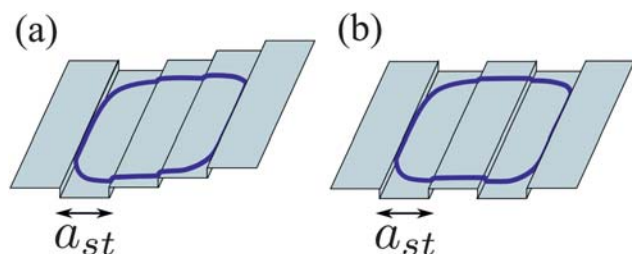


**Fig. 5** Adsorbed polymer ring on two periodic stripe patterns (a) and (b) consisting of several equidistant topographical surface steps with distance  $a_{st}$ . On both patterns (a) and (b), the ring is shown in configuration  $\Pi_0^2$  connecting two surface steps at distance  $3a_{st}$ . For small surface step heights both configurations are approximately identical.

elongated shapes  $\Pi_0^n$  where the ring binds to two surface steps  $i$  and  $i+n$  (shape  $\Pi_0^1$  is identical to shape  $\Pi_0$ ). All shapes  $\Pi_0^n$  can be approximated by two semicircles of diameter  $na_{st}$ , connected by two straight adhered segments of length  $L_{st} = L - n\pi a_{st}$ , which gives a total energy

$$\bar{E}_{\Pi_0^n} \approx 2\pi/n - |w_{st}|(\bar{L} - n\pi) \quad (22)$$

For a ring of contour length  $L$ , only states with  $n \leq n_{max} = \lceil \bar{L}/\pi \rceil$  are accessible. At small  $|w_{st}|$  the round shape I is stable. The criterion  $\bar{E}_I = \bar{E}_{\Pi_0^{n_{max}}}$  gives a first transition at

$$|w_{I-\Pi_0^{n_{max}}}| \approx \frac{2\pi}{\bar{L}n_{max}} \quad (23)$$

from shape I into shape  $\Pi_0^{n_{max}}$ . The criterion  $\bar{E}_{\Pi_0^{n+1}} = \bar{E}_{\Pi_0^n}$  gives a cascade of  $n_{max} - 1$  further morphological transitions from shape  $\Pi_0^{n+1}$  into shape  $\Pi_0^n$  at adhesion strengths

$$|w_{\Pi_0^n - \Pi_0^{n-1}}| \approx \frac{2}{n(n-1)} \quad (2 \leq n \leq n_{max}) \quad (24)$$

which are *independent* of the contour length  $L$ . For strong adhesion  $|w_{st}| > |w_{\Pi_0^2 - \Pi_0^1}| = 1$ , shape  $\Pi_0^2$  remains the ground state.

In the limit  $|w_{st}| \gg 1$ , the contact radius becomes small compared to the distance  $a_{st}$  between surface steps such that shapes  $\Pi_0^n$  become effectively kinked with sharp bends. According to the result (24), only shape  $\Pi_0^1$  connecting neighboring surface steps is stable in this limit and, thus, sharp kinks should be observable only for this shape.

We summarize our findings in a morphology diagram in Fig. 6 using the control parameters  $\bar{L}$  and  $|w_{st}|$  in Fig. 6(a) or  $\bar{L}$  and  $|W_{st}|L^2/\kappa = |w_{st}|\bar{L}^2$  in Fig. 6(b). Changing the adhesion strength  $|w_{st}|$  corresponds to horizontal paths in Fig. 6(a,b) and results in a cascade of transitions between different shapes  $\Pi_0^n$ . The same transition cascade is encountered when changing the surface step spacing and thus  $\bar{L} = L/a_{st}$  corresponding to a vertical line in Fig. 6(b).

For periodic stripe structures thermal fluctuations can play an important role. As discussed already for the surface groove they

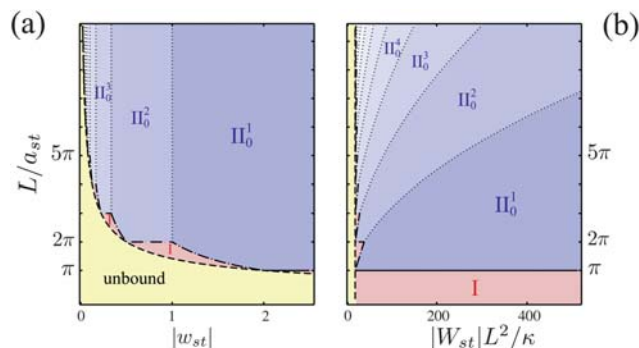


**Fig. 6** Morphology diagrams of a ring adhering to a substrate with  $n$  equidistant surface topographical steps at distance  $a_{st}$  as a function of (a) the contour length  $L/a_{st}$  and the reduced potential strength  $|w_{st}|$  as defined in (4) and (b)  $L/a_{st}$  and  $|W_{st}|L^2/\kappa = |w_{st}|\bar{L}^2/a_{st}^2$ . Shapes  $\Pi_0^n$  with  $n \geq 2$  represent elongated rings which bind to two surface steps that are separated by  $n$  terraces: the stability regimes of these shapes are shown in different colors of blue. The dashed line marks the unbinding transition, and the dot-dashed and dotted lines indicate the morphological transitions as estimated in eqn (23) and (24), respectively.



can give rise to a complete thermal unbinding from individual surface steps such that no morphological transitions can be observed below the critical reduced adhesion strength  $|w_{st,c}|$ , see eqn (16). For a periodic stripe pattern, all morphological transitions  $|w_{\Pi_0^n - \Pi_0^{n-1}}| \sim 1/n^2$  with  $n < |w_{st,c}|^{-1/2}$  should be observable before thermal unbinding happens. As discussed above we find  $|w_{st,c}| \ll 1$  for small polymer diameters and sufficiently large distances  $a_{st} \gg \ell^{1/3} L_p^{2/3}$  between surface steps.

Another effect of thermal fluctuations are *additional* kink-like excitations connecting neighboring surface steps.<sup>10,11,23,24</sup> In the absence of thermal fluctuations such kink excitations are absent as they cost an additional kink energy  $E_{\text{kink}}$ . Thermal fluctuations create kinks with an average density

$$\rho_{\text{kink}} \sim e^{-E_{\text{kink}}/T} = e^{-\bar{E}_{\text{kink}} L_p / 2a_{st}} \quad (25)$$

along the ring contour.<sup>24</sup>

If step distances are small compared to the contact radius,  $a_{st} \ll R_{co} = (\kappa/2|W_{st}|)^{1/2}$  or  $|w_{st}| \ll 1$ , the kink is elongated with a length  $L_{\text{kink}} \sim a_{st}^{1/2} R_{co}^{1/2} \sim a_{st}|w_{st}|^{-1/4}$  along the surface steps. The kink energy is  $E_{\text{kink}} \sim a_{st}^{1/2} \kappa^{1/4} |W_{st}|^{3/4}$  or  $\bar{E}_{\text{kink}} \sim |w_{st}|^{3/4}$  in this regime.<sup>23,24</sup> Therefore the thermal kink density is exponentially low according to eqn (25) if  $|w_{st}| \gg (a_{st}/L_p)^{4/3}$ , and kinks do not modify morphological transitions  $|w_{\Pi_0^n - \Pi_0^{n-1}}| \sim 1/n^2$  with  $n < (L_p/a_{st})^{2/3}$ . For persistence lengths much larger than the step distances,  $L_p/a_{st} \gg 1$ , a large cascade of transitions should remain observable. According to eqn (23) and (24) most of the morphological transitions for the periodic stripe pattern take place in the regime  $|w_{st}| \ll 1$  corresponding to  $a_{st} \ll R_{co}$ .

If step distances are large compared to the contact radius,  $a_{st} \gg R_{co}$  or  $|w_{st}| \gg 1$ , the kink crosses the potential barrier of width  $a_{st}$  in a right angle with two small curved segments of contact radius  $R_{co}$  connecting to the surfaces edges.<sup>†</sup> This gives rise to a kink length  $L_{\text{kink}} \sim a_{st}$  and a kink energy  $E_{\text{kink}} \sim a_{st}|W_{st}|$  or  $\bar{E}_{\text{kink}} \sim |w_{st}| \gg 1$ . Also in this regime the thermal kink density is exponentially low according to eqn (25) for persistence lengths much larger than the step distances,  $L_p/a_{st} \gg 1$ .

## 5 Ring condensation

Finally, our model is applied to the condensation transition of semiflexible polymer rings in poor solvent or in the presence of condensing agents giving rise an effective polymer-polymer attraction with a condensation energy gain  $W_{\text{con}} < 0$  per contact length.

For small condensation energies, the semiflexible ring will remain in a round ring configuration with its total energy given by the bending energy

$$E_{\text{ring}} = E_{b,\text{ring}} = 2\pi^2 \kappa / L \quad (26)$$

For strong attractive interactions between polymer segments, one expects the polymer ring to form a toroid, similar to open polymers.<sup>12,13</sup> The radius of the toroid will be  $L/2\pi n$ , where  $n$  is the winding number and  $L$  the contour length of the ring. In comparison to the ring adsorbed to the stripe structures, the length scale of the stripe width is absent, and the morphologies in the presence of a condensing potential are characterized by only

<sup>†</sup> In ref. 10,11 such kink excitations have been called ‘‘crossings’’.



**Fig. 7** Metastable racquet shape of a condensed ring. Segments that adhere to each other are colored in blue.

one parameter, namely  $|W_{\text{con}}|L^2/\kappa$  (if  $L_p$  is large such that thermal unbinding can be neglected<sup>21</sup>). The total energy of a toroidal configuration with winding number  $n = 2$  is

$$E_{\text{tor}} = \frac{\kappa}{2L} \left( 16\pi^2 - \frac{|W_{\text{con}}|L^2}{\kappa} \right) \quad (27)$$

For toroids with  $n > 2$  the packing structure, which is commonly assumed to be hexagonal,<sup>12–15</sup> has to be taken into account.

Comparing the energies of toroids and rings, we find that a discontinuous transition from a ring to the first condensed toroidal state with  $n = 2$  windings occurs at  $|W_{\text{con,tor}}|L^2/\kappa = 12\pi^2$ .

Finally the ring can also assume racquet-shaped metastable configurations as shown in Fig. 7, which resemble the elongated shapes  $\Pi_2$  containing two bulges. Performing a similar calculation as for the bulged shapes, which is contained in appendix, we can calculate the total energy of the racquet shapes as

$$E_{\text{tot,rac}} = \frac{\kappa}{2L} \left( 12.85 \left( \frac{|W_{\text{con}}|L^2}{\kappa} \right)^{1/2} - \frac{1}{2} \frac{|W_{\text{con}}|L^2}{\kappa} \right) \quad (28)$$

which is valid for  $|W_{\text{con}}|L^2/\kappa > 73.33$  sufficiently large that the contact length is nonzero. Comparing with the energy (27) of the toroidal configurations, we find that the racquet shape has a higher energy for  $|W_{\text{con}}|L^2/\kappa > 82.49$ , *i.e.*, for all  $|W_{\text{con}}| > |W_{\text{con,tor}}|$ . Comparing with the energy (26) of the uncondensed ring, we find that the racquet shape has a higher energy for  $|W_{\text{con}}|L^2/\kappa < 578.34$ , *i.e.*, for all  $|W_{\text{con}}| < |W_{\text{con,tor}}|$ . Therefore, either the uncondensed ring or the toroidal configuration represent the global energy minimum, and racquet-like shapes are only metastable configurations in ring condensation. In contrast, the analogous bulged elongated shapes  $\Pi_2$  can represent globally stable states of semiflexible rings adsorbed on striped substrates.

## 6 Conclusion

We showed that morphologies of adsorbed semiflexible polymer ring on a substrate containing an adhesive stripe domain can be completely classified. Whereas a flexible polymer ring assumes a random coil configurations, which can easily adapt its shape to fit into the adhesive stripe as long as the persistence length of the flexible polymer is much smaller than the stripe width, the bending energy of a semiflexible polymer ring leads to the existence of only four distinct metastable states as shown in Fig. 1: A round toroidal configuration I, a confined elongated shape II, as well as two shapes  $\Pi_1$  and  $\Pi_2$  containing one or two bulges, respectively.

Specifically we considered two types of adhesive stripe domains, topographical surface grooves and chemically structured surface domains. Both types of structures lead to very similar behavior: a *discontinuous morphological transition* between the two dominant shapes I and  $\Pi_0$ , as well as

intermediate bulge shapes  $\Pi_1$  and  $\Pi_2$  for large contour lengths, of which only shape  $\Pi_2$  containing two bulges can be globally stable.

Estimates for all transition lines were derived, see Fig. 4, which could serve to determine material properties of the substrate or the polymer ring experimentally. The discontinuous transitions display shape hysteresis and are observable for persistence lengths exceeding the stripe width.

For a periodic array of topographic steps we find a cascade of morphological shape transitions as displayed in Fig. 6.

## Appendix

### A Analytical energy minimization for topographical surface steps

In this appendix we derive exact analytical results for the metastable shapes of a ring adhering to a topographical surface groove with two adhesive edges. All four metastable ring shapes consist of one or two straight segments (with tangent angles  $\theta(s) = 0$  or  $\theta(s) = \pi$ ) of total length  $L_{st}$ , which adhere to the straight stripe edges and one or two curved segments of total length  $L - L_{st}$ . The total energy of the ring is

$$E_{\text{tot}}(L_{st}) = E_b(L_{st}) - |W_{st}|L_{st} \quad (29)$$

Only the curved segments contribute to the bending energy  $E_b = (\kappa/2) \int_0^L ds (\partial_s \theta(s))^2$ , whereas only the straight adhered segment contribute to the adhesion energy  $E_{ad} = -|W_{st}|L_{st}$ .

For each shape additional constraints have to be imposed for ring closure, which take on slightly different forms for the shapes of type I adhering to one edge and shapes II adhering to both edges of the stripe.

The total energy is minimized with respect to variations of the tangent angle configuration  $\theta(s)$  with  $0 \leq s \leq L$ . For each metastable shape we first minimize the bending energy under the additional constraint of fixed adhered length  $L_{st}$  to obtain the constrained bending energy minimum  $E_b = E_b(L_{st})$  as a function of  $L_{st}$ . Then we minimize the total energy (29) also with respect to  $L_{st}$  to obtain the unconstrained minimal energy  $E_{\text{tot}} = E_{\text{tot}}(W_{st})$  as a function of  $|W_{st}|$ , which is equivalent to a Legendre transform of the bending energy  $E_b(L_{st})$  with respect to the adhered length  $L_{st}$ . We obtain exact results for energy minima  $E_b = E_b(L_{st})$  and  $E_{\text{tot}} = E_{\text{tot}}(W_{st})$  in

parametric form and can solve for explicit formulae in the limits of strong and weak adhesion.

**A.1 Shape I.** Shape I contains one round segment of length  $L_r$  and one adhered segment with  $L_r + L_{st} = L$ . Shape I is parameterized with one half of the curved segment at arc lengths  $0 \leq s \leq L_r/2$  as shown in Fig. 8(a). Considering one half of the symmetric configuration, the ring closure constraint for the coordinate parallel to the groove can be written as

$$\int_0^{L_r/2} ds \cos \theta(s) + \frac{L_{st}}{2} = 0 \quad (30)$$

We associate this constraint with a Lagrange multiplier  $\mu$ . The resulting Euler–Lagrange equation minimizing the bending energy of the round segment is

$$\kappa \partial_s^2 \theta + \mu \sin \theta = 0 \quad (31)$$

Integrating once we find

$$\frac{\kappa}{2} (\partial_s \theta)^2 - \mu \cos \theta = c$$

$$ds = d\theta \left[ \frac{2\mu}{\kappa} (q + \cos \theta) \right]^{-1/2} \quad (32)$$

with an integration constant  $c$  and the parameter  $q \equiv c/\mu$ . We have two equations for the two unknown parameters  $q$  and  $\mu$ : The first equation gives the length of the round segment

$$L_r = L - L_{st} = 2 \left( \frac{2\kappa}{\mu} \right)^{1/2} f_1(q)$$

$$f_1(q) \equiv \int_0^\pi d\theta (q + \cos \theta)^{-1/2} \quad (33)$$

The second equation is given by the constraint (30)

$$L_{st} = 2 \left( \frac{2\kappa}{\mu} \right)^{1/2} f_2(q)$$

$$f_2(q) \equiv - \int_0^\pi d\theta \cos \theta (q + \cos \theta)^{-1/2} \quad (34)$$

The functions  $f_1(q)$  and  $f_2(q)$  can be expressed by elliptic integrals, which converge for  $q > 1$ .

Instead of solving explicitly for  $q$  and  $\mu$ , we will express all quantities of interest parametrically as functions of  $q$  using the two eqn (33) and (34). This gives

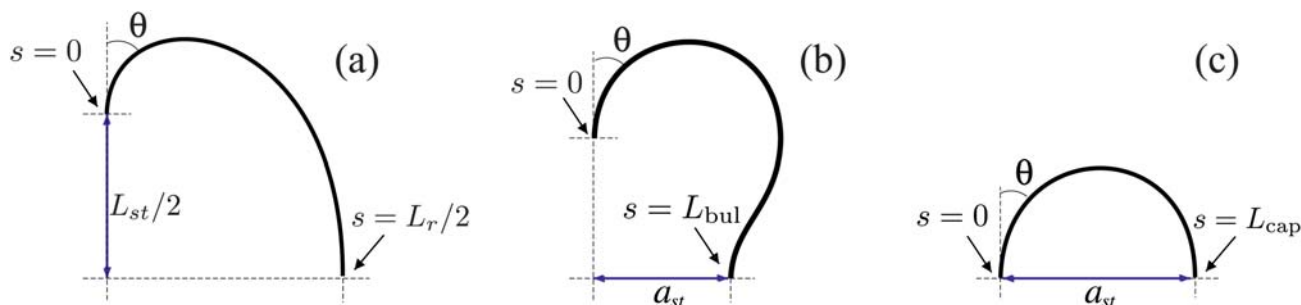


**Fig. 8** Shapes I,  $\Pi_0$ ,  $\Pi_1$  and  $\Pi_2$  in Fig. 1(a) can be divided into straight (adsorbed) segments of total length  $L_{st}$  and curved (desorbed) segments of the three types shown in this figure. Configuration I consists of two curved segments as shown in (a). Shape  $\Pi_0$ , consists of two straight segment and two unbulged caps as shown in (c). Shape  $\Pi_1$  consists of two straight segments and one bulged cap as shown in (b) and on unbulged cap as shown in (c). Shape  $\Pi_2$  consists of two straight segments and two bulged caps as shown in (b).

$$\frac{L_{st}}{L} = 1 - \frac{L_r}{L} = \frac{f_2(q)}{f_1(q) + f_2(q)} \quad (35)$$

$$\frac{2\mu L^2}{\kappa} = 4(f_1(q) + f_2(q))^2 \quad (36)$$

In addition, the bending energy can be rewritten as

$$\begin{aligned} E_b &= (2\kappa\mu)^{1/2} f_3(q) \\ f_3(q) &\equiv \int_0^\pi d\theta (q + \cos\theta)^{1/2} \end{aligned} \quad (37)$$

where also the function  $f_3(q)$  can be expressed by elliptic integrals. It follows that the bending energy is given by

$$\frac{E_b L}{\kappa} = 2(f_1(q) + f_2(q)) f_3(q) \quad (38)$$

Eqn (38) and (35) give a parametric representation of  $E_b(L_{st})$  using the parameter  $q > 1$ . The corresponding curve is shown in Fig. 2(a) as red line.

For  $q \approx 1$ , both  $f_1(q)$  and  $f_2(q)$  diverge while  $f_1(q) - f_2(q) \approx f_3(q) \approx 2\sqrt{2}$ , such that  $L_{st} \approx L/2$  and

$$\frac{E_b L}{\kappa} \approx 8L(L/2 - L_{st})^{-1} \quad (39)$$

diverges corresponding to the limit of maximal adhered length and an maximally elongated ring configuration. In the limit of large  $q \gg 1$ , we find  $f_1(q) \approx \pi q^{-1/2}$ ,  $f_2(q) \approx \pi q^{-3/2}$ , and  $f_3(q) \approx \pi q^{1/2}$  such that  $L_{st} \approx 0$  and  $E_b L/\kappa \approx 2\pi^2$  corresponding to a circular ring adhering in a single point.

If the constraint of fixed adhered length  $L_{st}$  is lifted, we have to minimize the total energy (29) also with respect to variations of  $L_{st}$ . This gives a transversality condition for the contact curvature at each contact point where a curved segment joins the straight adhered segments

$$|\partial_s \theta(s_{co})| = \frac{1}{R_{co}} = \left( \frac{2|W_{st}|}{\kappa} \right)^{1/2} \quad (40)$$

Using this condition in (32) we find  $c = |W_{st}| - \mu$  or

$$q = \frac{|W_{st}|}{\mu} - 1 \quad (41)$$

which allows us to express also  $|W_{st}|$  as a function of the parameter  $q$  using (36),

$$\frac{|W_{st}| L^2}{\kappa} = 2(q+1)(f_1(q) + f_2(q))^2 \quad (42)$$

and to obtain together with (38) and (35) a parametric representation of  $E_{tot}(|W_{st}|)$  using the parameter  $q$ . The corresponding curve is shown in Fig. 3(a,b) as red line.

The limiting case  $q \approx 1$  with  $L_{st} \approx L/2$  corresponds to adhesion strengths  $|W_{st}| L^2/\kappa = L^2/2R_{co}^2 \gg 2\pi^2$ . Using the asymptotics of the functions  $f_i(q)$  we find

$$\frac{E_{tot,1} L}{\kappa} \approx 4\sqrt{2} \left( \frac{|W_{st}| L^2}{\kappa} \right)^{1/2} - \frac{1}{2} \frac{|W_{st}| L^2}{\kappa} \quad (43)$$

in this limit. Large  $q \gg 1$  with  $L_{st} \approx 0$  corresponds to  $|W_{st}| L^2/\kappa \approx 2\pi^2$ , which is the critical value for the unbinding transition from a single surface step, which is also known for vesicles adhering to a surface.<sup>19,20</sup> In the vicinity of this critical value we find

$$\frac{E_{tot,1} L}{\kappa} \approx 2\pi^2 - \frac{1}{24\pi^2} \left( \frac{|W_{st}| L^2}{\kappa} - 2\pi^2 \right)^2 \quad (44)$$

which shows that the unbinding transition is *continuous*. The asymptotic estimate (43) is shown in Fig. 3(a) as dashed line.

**A.2 Shape  $\Pi_0$ .** Shape  $\Pi_0$  consists of two round caps of lengths  $L_{cap,1}$  and  $L_{cap,2}$  and two adhered segments with total length  $L_{st}$  such that  $L_{cap,1} + L_{cap,2} + L_{st} = L$ . The caps have reflection symmetry with respect to the axis  $x = a_{st}/2$ . The ring closure constraints for the coordinate perpendicular to the groove ensure that the curved segments connect both groove edges,

$$\int_{L_{cap,i}} ds \sin\theta(s) - a_{st} = 0 \quad (45)$$

for each cap  $i = 1, 2$ . The constraints are associated with Lagrange multipliers  $\nu_i$ . The Euler Lagrange equations for the shape of the caps become

$$\kappa \partial_s^2 \theta - \nu_i \cos \theta = 0 \quad (46)$$

Integrating once we find

$$\begin{aligned} \frac{\kappa}{2} (\partial_s \theta)^2 - \nu_i \sin \theta &= c_i \\ ds &= d\theta \left[ \frac{2\nu_i}{\kappa} (p_i + \sin \theta) \right]^{-1/2} \end{aligned} \quad (47)$$

with integration constants  $c_i$  and parameters  $p_i \equiv c_i/\nu_i$ . In total we have to determine six unknown parameters  $L_{cap,i}$ ,  $p_i$ , and  $\nu_i$ . These parameters have to fulfill four equations

$$\begin{aligned} 2L_{cap,i} &= \left( \frac{2\kappa}{\nu_i} \right)^{1/2} g_1(p_i) \\ g_1(p) &\equiv \int_0^\pi d\theta (p + \sin \theta)^{-1/2} \end{aligned} \quad (48)$$

for the cap lengths and

$$\begin{aligned} a_{st} &= 2 \left( \frac{\kappa}{2\nu_i} \right)^{1/2} g_2(p_i) \\ g_2(p) &\equiv - \int_0^\pi d\theta \sin \theta (p + \sin \theta)^{-1/2} \end{aligned} \quad (49)$$

for the constraints (45), The functions  $g_1(p)$  and  $g_2(p)$  can be expressed by elliptic integrals, which converge for  $p > 0$  and  $p < -1$ . Note that for  $p < -1$  the functions  $g_1(p)$  and  $g_2(p)$  are imaginary.

In addition the cap lengths have to fulfill  $L_{cap,1} + L_{cap,2} + L_{st} = L$ . A sixth equation arises because the two caps can exchange length while the adhered length  $L_{st}$  stays fixed. This leads to the additional transversality condition that the contact curvatures of the two caps have to be equal. This condition enforces that both caps are *identical*: Because at all four contact points  $\sin \theta(s_{co}) = 0$ , the Euler Lagrange eqn (47) lead to equal integration constants  $c_i$  are equal for both caps,  $c \equiv c_1 = c_2$  or  $\nu_i = c/p_i$ . Together with the two equations for the constraints (49) it follows that  $p \equiv p_1 = p_2$ . Therefore, both caps are identical and also have the same size  $L_{cap} = L_{cap,1} = L_{cap,2}$ . As a result we are left with two parameters  $p$  and  $\nu$  to be determined with  $L_{cap}$  fixed by  $2L_{cap} = L - L_{st}$  for a prescribed adhered length.



Instead of explicitly solving for  $p$  and  $\nu$ , we express all quantities of interest as functions of  $p$  using (48) and (49):

$$\bar{L}_{\text{cap}} = \frac{L_{\text{cap}}}{a_{st}} = \frac{g_1(p)}{g_2(p)} \quad (50)$$

$$\bar{L}_{st} = \frac{L_{st}}{a_{st}} = \bar{L} - \frac{2g_1(p)}{g_2(p)} \quad (51)$$

$$\frac{\nu a_{st}^2}{\kappa} = \frac{1}{2} g_2(p)^2 \quad (52)$$

The bending energy of the caps becomes

$$E_b = 2E_{\text{cap}} = (2\kappa\nu)^{1/2} g_3(p) \quad (53)$$

$$g_3(p) \equiv \int_0^\pi d\theta (p + \sin\theta)^{1/2}$$

where the function  $g_3(p)$  can be expressed by elliptic integrals. For  $p < -1$  all three functions  $g_i(p)$  are imaginary but physical quantities remain real-valued. It follows that

$$\bar{E}_b = \frac{E_b a_{st}}{\kappa} = g_2(p) g_3(p) \quad (54)$$

which gives together with (51) a parametric representation of  $E_b(L_{st})$  using the parameter  $p$  in the range  $p > 0$  and  $p < -1$ . The corresponding curve is shown in Fig. 2(a) as blue line.

For  $p \approx -1$  both  $g_1(p)$  and  $g_2(p)$  diverge on the negative imaginary axis, whereas  $g_3(-1) \approx -i4(\sqrt{2}-1)$  such that  $\bar{L}_{st} \approx \bar{L} - 2$  or  $L_{\text{cap}} \approx a_{st}$  corresponding to the limit of maximal adhered length and a ring configuration approaching a rectangular shape. Accordingly  $E_b$  diverges in this limit,

$$\bar{E}_b = 2\bar{E}_{b,\text{cap}} \approx 32(\sqrt{2}-1)^2 (\bar{L} - 2 - \bar{L}_{st})^{-1} \quad (55)$$

For  $p \gg 1$  (and similarly for  $p \ll -1$ ), we have  $g_1(p) \approx \pi p^{-1/2}$ ,  $g_2(p) \approx \pi p^{-1/2}$ , and  $g_3(p) \approx \pi p^{1/2}$  such that  $\bar{L}_{st} \approx \bar{L} - \pi$  or  $L_{\text{cap}} \approx \pi a_{st}/2$  corresponding to exactly semicircular caps with radius  $R_{co} = a_{st}/2$ . The bending energy is

$$\bar{E}_b = 2\bar{E}_{\text{cap}} \approx 2\pi \quad (56)$$

For  $p \approx 0$ , finally, the caps become very elongated with large contact radius  $R_{co}$  and  $g_1(0) \approx 5.24$ ,  $g_2(0) = g_3(0) \approx 2.40$  such that the adhered length assumes its minimal value  $\bar{L}_{st} \approx \bar{L} - 4.38$  or  $\bar{L}_{\text{cap}} \approx 2.19$ , and the bending energy becomes

$$\bar{E}_b = 2\bar{E}_{b,\text{cap}} \approx 5.74 \quad (57)$$

If the constraint of fixed adhered length  $L_{st}$  is lifted the transversality condition of contact curvature at the contact points gives  $c = |W_{st}|$  or

$$p = \frac{|W_{st}|}{\nu} \quad (58)$$

which leads to

$$|W_{st}| = \frac{|W_{st}| a_{st}^2}{\kappa} = \frac{1}{2} p g_2^2(p) \quad (59)$$

Together with (54) this gives a parametric representation of  $\bar{E}_{\text{tot}}(|W_{st}|)$  using the parameter  $p$  in the range  $p > 0$  and  $p < -1$ . The corresponding curve is shown in Fig. 3(a,b) as blue line.

The limiting case  $p \approx -1$  with  $\bar{L}_{st} \approx \bar{L} - 2$  corresponds to strong adhesion with  $|w_{st}| \gg 2$  and

$$\bar{E}_{\text{tot},\text{II}_0} \approx 8\sqrt{2}(\sqrt{2}-1)|w_{st}|^{1/2} - |w_{st}|(\bar{L}-2) \quad (60)$$

For  $|p| \gg 1$  we find intermediate adhesion strengths  $|w_{st}| \approx 2$  and

$$\bar{E}_{\text{tot},\text{II}_0} \approx 2\pi - |w_{st}|(\bar{L} - \pi) \quad (61)$$

The limiting case  $p \approx 0$  with  $\bar{L}_{st} \approx \bar{L} - 4.38$  corresponds to weak adhesion with  $|w_{st}| \ll 1$  and

$$\bar{E}_{\text{tot},\text{II}_0} \approx 5.74 - |w_{st}|(\bar{L} - 4.38) - 1.31|w_{st}|^{3/2} \quad (62)$$

The asymptotic estimate (62) is shown in Fig. 3(a) as dashed line.

**A.3 Shape II<sub>2</sub>.** Shape II<sub>2</sub> consists of two bulges of lengths  $L_{\text{bul},1}$  and  $L_{\text{bul},2}$  and two adhered segments with total length  $L_{st}$  and  $L_{\text{bul},1} + L_{\text{bul},2} + L_{st} = L$ . As opposed to the caps of shape II<sub>0</sub> bulges have no reflection symmetry. Also the bulges of shape II<sub>2</sub> can exchange length with the adhered length  $L_{st}$  fixed. As for the caps, this leads to a transversality constraint that curvatures at contact points connected by an adhered segment have to be equal. Using analogous arguments as for caps in shape II<sub>0</sub> this leads to the conclusion that both bulges must be identical in size,  $L_{\text{bul}} = L_{\text{bul},1} = L_{\text{bul},2}$ . The bulge length is fixed by  $2L_{\text{bul}} = L - L_{st}$  for a prescribed adhered length.

There are two energetically degenerate configurations of the two bulges in shape II<sub>2</sub>: An arrangement with reflection symmetry with respect to the  $y$ -axis and both bulges on the same side of the stripe, and an antisymmetric arrangement with both bulges on opposite sides.

The ring closure constraint for the coordinate perpendicular to the groove is

$$\int_{L_{\text{bul}}} ds \sin\theta(s) - a_{st} = 0 \quad (63)$$

which we associate with a Lagrange multiplier  $\nu$ . The Euler Lagrange equations and their first integral are identical to eqn (46) and (47) for the shape II<sub>0</sub>, the integration constant  $c$  also defines a parameter  $p \equiv c/\nu$ . The two unknown parameters  $p$  and  $\nu$  are determined by the two equations

$$2L_{\text{bul}} = L - L_{st} = \left(\frac{2\kappa}{\nu}\right)^{1/2} h_1(p) \quad (64)$$

$$h_1(p) \equiv \left( \int_0^\pi + 2 \int_\pi^{\theta_{\text{inf}}} \right) d\theta (p + \sin\theta)^{-1/2}$$

for the bulge length and

$$a_{st} = 2 \left(\frac{\kappa}{2\nu}\right)^{1/2} h_2(p) \quad (65)$$

$$h_2(p) \equiv - \left( \int_0^\pi + 2 \int_\pi^{\theta_{\text{inf}}} \right) d\theta \cos\theta (p + \sin\theta)^{-1/2}$$

for the constraint (63). Here,  $\theta_{\text{inf}}$  is the tangent angle in the inflection point of the bulge configuration, see Fig. 8(c). It is determined from  $\partial_s \theta_{\text{inf}} = 0$  which gives  $\theta_{\text{inf}} = \arcsin(-p)$  with  $\pi < \theta_{\text{inf}} < 3\pi/2$ , which restricts  $p$  to  $0 < p < 1$ . Also the functions  $h_1(p)$  and  $h_2(p)$  can be expressed by elliptic integrals. The

function  $h_2(p)$  becomes negative for  $p > p_\infty \approx 0.652$ , which restricts  $p$  to  $0 < p < p_\infty$ .

We express all quantities of interest as functions of  $p$  using (64) and (65):

$$\bar{L}_{\text{bul}} = \frac{L_{\text{bul}}}{a_{st}} = \frac{h_1(p)}{h_2(p)} \quad (66)$$

$$\bar{L}_{st} = \frac{L_{st}}{a_{st}} = \bar{L} - \frac{2h_1(p)}{h_2(p)} \quad (67)$$

$$\frac{\nu a_{st}^2}{\kappa} = \frac{1}{2} h_2(p)^2 \quad (68)$$

According to (66) the length of the bulge diverges for  $p \approx p_\infty$  as  $\bar{L}_{\text{bul}} \approx 5.72/(p_\infty - p)$ . Therefore, we can determine a  $\bar{L}$ -dependent value  $p_L(\bar{L}) < p_\infty$  such that  $\bar{L}_{st} < 0$  for  $p > p_L(\bar{L})$ , which sets the range  $0 < p < p_L(\bar{L})$  of accessible bulged states for a ring of finite length. For very large  $\bar{L}$ ,  $p_L(\bar{L}) \approx p_\infty$ . For  $\bar{L} = 20$  as in Fig. 2 and 3, we find  $p_L \approx 0.53$ .

The bending energy can be rewritten as

$$E_b = 2E_{b,\text{bul}} = (2\kappa\nu)^{1/2} h_3(p) \quad (69)$$

$$h_3(p) \equiv \left( \int_0^\pi + 2 \int_\pi^{\theta_{\text{mf}}} \right) d\theta (p + \sin\theta)^{1/2}$$

where also the function  $h_3(p)$  can be expressed by elliptic integrals. It follows that

$$\bar{E}_b = \frac{E_b a_{st}}{\kappa} = h_2(p) h_3(p) \quad (70)$$

which gives together with (67) a parametric representation of  $E_b(L_{st})$  using the parameter  $p$  in the range  $0 < p < p_L(\bar{L})$  of accessible parameters  $p$ . The corresponding curve is shown in Fig. 2(a) as green line.

For  $p \approx 0$  the bulge of shape  $\text{II}_2$  approaches the maximally elongated cap of shape  $\text{II}_0$ , and the adhered length approaches the above result  $\bar{L}_{st} \approx \bar{L} - 4.38$  or  $\bar{L}_{\text{bul}} = \bar{L}_{\text{cap}} \approx 2.19$  with a bending energy  $\bar{E}_b = 2\bar{E}_{b,\text{bul}} \approx 5.74$ .

If the constraint of fixed adhered length  $L_{st}$  is lifted the condition of contact curvature at the contact points gives  $c = |W_{st}|$  or

$$p = \frac{|W_{st}|}{\nu} \quad (71)$$

which leads to

$$|w_{st}| = \frac{1}{2} p h_2^2(p) \quad (72)$$

This relation gives a maximal value  $|w_{st}| = w_{\text{max}} \approx 0.35$  which is realized for  $p = p_{\text{max}} \approx 0.25$ . For  $|w_{st}| > w_{\text{max}}$ , eqn (72) has no solution because bulged shapes  $\text{II}_2$  are no longer metastable states and are unstable with respect to transitions into shape  $\text{II}_0$ . For  $|w_{st}| < w_{\text{max}}$ , there are two solutions  $p$  to eqn(72). The solution branch with  $p > p_{\text{max}}$  corresponds to the local energy minimum representing shape  $\text{II}_2$  whereas the solution branch with  $p < p_{\text{max}}$  corresponds to a local maximum of the total energy and, thus, represents a possible transition state  $\text{II}_2^*$  for shape transitions into shapes  $\text{II}_1$  or  $\text{II}_0$ . This maximum corresponds to a shape with two identical *small* bulges which are unstable with

respect to shrinking to zero size to a shape  $\text{II}_0$  or to expanding to its equilibrium size in state  $\text{II}_2$ . Eqn (72) and (70) give a parametric representation of  $\bar{E}_{\text{tot}}(|w_{st}|)$  for a metastable shape  $\text{II}_2$  using the parameter  $p$  in the range  $p_{\text{max}} < p < p_L(\bar{L})$ . The value  $p = p_L(\bar{L})$  corresponds to a minimal value  $|w_{st}| = w_{\text{min}}(\bar{L})$ , which is  $\bar{L}$ -dependent. For  $|w_{st}| > w_{\text{min}}$ , bulged shapes  $\text{II}_2$  become unstable with respect to transitions into shape I because bulged become so large that the adhered length  $\bar{L}_{st}$  vanishes. For  $\bar{L} = 20$  we find  $w_{\text{min}} \approx 0.10$ . The corresponding curve is shown in Fig. 3(a,b) for  $\bar{L} = 20$  as green line in the corresponding range  $w_{\text{min}} < |w_{st}| < w_{\text{max}}$ . For the range  $0 < p < p_{\text{max}}$  the parametric representation gives the additional branch of transition states  $\text{II}_2^*$  shown in Fig. 3(b) as green dashed line in the corresponding range  $0 < |w_{st}| < w_{\text{max}}$ .

For  $p \approx p_\infty$  the bulge length diverges. This limit corresponds to weak adhesion with  $|w_{st}| \ll 1$ . Expanding the functions  $h_i(p)$  around  $p \approx p_\infty$  we find

$$\bar{L}_{\text{bul}} \approx |w_{st}|^{-1/2} \left( 3.75 - 1.53 |w_{st}|^{1/2} - 0.54 |w_{st}| \right)$$

$$\bar{E}_{b,\text{bul}} \approx |w_{st}|^{1/2} (3.75 + 0.18 |w_{st}|)$$

$$\bar{E}_{\text{tot},\text{II}_2} \approx 15.00 |w_{st}|^{1/2} - |w_{st}| (\bar{L} + 3.07) - 0.72 |w_{st}|^{3/2} \quad (73)$$

This asymptotic estimate is shown in Fig. 3(a) for  $\bar{L} = 20$  as dashed line in the accessible range  $p_{\text{max}} < p < p_L(\bar{L})$  corresponding to  $0.10 < |w_{st}| < w_{\text{max}}$ .

We can also define an energy  $\Delta\bar{E}_{\text{bul}}$  for creating a bulge starting from the shape  $\text{II}_0$ . This energy includes the bending energy gain of a bulge as compared to a cap as well as the adhesion energy cost from desorbing additional length,

$$\Delta\bar{E}_{\text{bul}} = (E_{\text{tot},\text{II}_2} - E_{\text{tot},\text{II}_0})/2$$

$$\approx -2.87 + 7.50 |w_{st}|^{1/2} - 3.72 |w_{st}| + 0.30 |w_{st}|^{3/2} \quad (74)$$

where the last approximation holds for  $|w_{st}| \ll 1$ .

**A.4 Shape  $\text{II}_1$ .** Shape  $\text{II}_1$  consists of one bulge of length  $L_{\text{bul}}$ , one cap of length  $L_{\text{cap}}$ , and two adhered segments with total length  $L_{st}$  such that  $L_{\text{bul}} + L_{\text{cap}} + L_{st} = L$ . We have to consider bulge and cap separately and apply two constraints

$$\int_{L_{\text{bul}}} \sin \theta(s) - a_{st} = 0$$

$$\int_{L_{\text{cap}}} \sin \theta(s) - a_{st} = 0 \quad (75)$$

which we associate with two Lagrange multipliers  $\nu_{\text{bul}}$  and  $\nu_{\text{cap}}$ . The Euler Lagrange equations and their first integral are identical to eqn (46) and (47) for the shapes  $\text{II}_0$  and  $\text{II}_2$ . Because the adhered length between bulge and cap can be adjusted in shape  $\text{II}_1$  we have an additional transversality condition that the contact curvatures have to be equal. Because at all four contact points  $\sin \theta(s_{co}) = 0$ , the Euler Lagrange eqn (47) lead to the equivalent condition that the integration constants are equal for bulge and cap,  $c = c_{\text{bul}} = c_{\text{cap}}$ . We introduce two corresponding parameters  $p_1$  and  $p_2$  such that

$$c = p_1 \nu_{\text{bul}} = p_2 \nu_{\text{cap}} \quad (76)$$

This relation together with  $L_{\text{bul}} + L_{\text{cap}} + L_{\text{st}} = L$  and the four equations for cap and bulge length and constraints,

$$L_{\text{bul}} = \left(\frac{\kappa}{2\nu_{\text{bul}}}\right)^{1/2} h_1(p_1) \quad (77)$$

$$L_{\text{cap}} = \left(\frac{\kappa}{2\nu_{\text{cap}}}\right)^{1/2} g_1(p_2) \quad (78)$$

$$a_{\text{st}} = 2\left(\frac{\kappa}{2\nu_{\text{bul}}}\right)^{1/2} h_2(p_1) \quad (79)$$

$$a_{\text{st}} = 2\left(\frac{\kappa}{2\nu_{\text{cap}}}\right)^{1/2} g_2(p_2) \quad (80)$$

give six equations for the six parameters  $L_{\text{bul}}$ ,  $L_{\text{cap}}$ ,  $p_1$ ,  $p_2$ ,  $\nu_{\text{bul}}$  and  $\nu_{\text{cap}}$ .

From these equations we find

$$\bar{L}_{\text{bul}} = \frac{h_1(p_1)}{h_2(p_1)}, \bar{L}_{\text{cap}} = \frac{g_1(p_2)}{g_2(p_2)}$$

$$p_1 h_2^2(p_1) = p_2 g_2^2(p_2) \quad (81)$$

Using the last equation we can solve numerically for  $p_2$  which allows us to express the adhered length  $L_{\text{st}} = L - L_{\text{bul}} - L_{\text{cap}}$  parametrically as a function of  $p_1$ . It follows that the adhered length of shape  $\text{II}_1$  with one bulge and one cap for given  $p_1$  and corresponding  $p_2$  is the mean value of the adhered lengths of shapes  $\text{II}_2$  with two bulges for  $p = p_1$  and  $\text{II}_0$  two caps for  $p = p_2$ ,

$$L_{\text{st},\text{II}_1}(p_1) = \frac{1}{2}(L_{\text{st},\text{II}_2}(p_1) + L_{\text{st},\text{II}_0}(p_2)) \quad (82)$$

Therefore, as for the shape  $\text{II}_2$ , the length of the bulge diverges for  $p_1 \approx p_\infty$ . There exists a  $\bar{L}$ -dependent value  $p_{1,L}(\bar{L}) < p_\infty$  such that the adhered length on one of the stripe edges shrinks to zero, which sets the range  $0 < p < p_{1,L}(\bar{L})$  of accessible bulged states for a ring of finite length. For very large  $\bar{L}$ ,  $p_{1,L}(\bar{L}) \approx p_\infty$ . For  $\bar{L} = 20$  as in Fig. 2 and 3, we find  $p_{1,L} \approx 0.55$ .

Furthermore the bending energy becomes

$$E_b = E_{\text{bul}} + E_{\text{cap}}$$

$$= (2\kappa\nu_{\text{bul}})^{1/2} h_3(p_1) + (2\kappa\nu_{\text{cap}})^{1/2} g_3(p_2) \quad (83)$$

Using (81) we can express also the bending energy parametrically as a function of  $p_1$ . The bending energy in shape  $\text{II}_1$  is given by the mean value of the bending energies of shapes  $\text{II}_2$  with two bulges for  $p = p_1$  and  $\text{II}_0$  two caps for  $p = p_2$ ,

$$E_{b,\text{II}_1}(p_1) = \frac{1}{2}(E_{b,\text{II}_2}(p_1) + E_{b,\text{II}_0}(p_2)) \quad (84)$$

Together with the parametric result for  $L_{\text{st}}$  we obtain a parametric representation of  $E_b(L_{\text{st}})$  using the parameter  $p_1$  in the range  $0 < p_1 < p_{1,L}(\bar{L})$  of accessible parameters  $p_1$ . The corresponding curve is shown in Fig. 2(a) as violet line.

If the constraint of fixed adhered length  $L_{\text{st}}$  is lifted the condition of contact curvature at the contact points gives  $c = |W_{\text{st}}|$  or

$$p_1 = \frac{|W_{\text{st}}|}{\nu_{\text{bul}}} \text{ and } p_2 = \frac{|W_{\text{st}}|}{\nu_{\text{cap}}} \quad (85)$$

which leads to

$$|w_{\text{st}}| = \frac{1}{2} p_1 h_2^2(p_1) = \frac{1}{2} p_2 g_2^2(p_2) \quad (86)$$

which is equivalent to the above relation (81) between  $p_1$  and  $p_2$ . It follows that for a given value of  $w_{\text{st}}$  the condition of the same contact curvature at all four contact points automatically leads to values  $p_1$  and  $p_2$  satisfying (81). According to (82) and (84), we conclude that the total energy of shape  $\text{II}_1$  is exactly the mean value of the total energies of shape  $\text{II}_0$  and shape  $\text{II}_2$ ,

$$E_{\text{tot},\text{II}_1} = \frac{1}{2}(E_{\text{tot},\text{II}_2} + E_{\text{tot},\text{II}_0})$$

$$= E_{\text{tot},\text{II}_0} + \Delta E_{\text{bul}} \quad (87)$$

for the same value of the adhesion strength  $w_{\text{st}}$ . The shape  $\text{II}_1$  exists for  $p_{\text{max}} < p_1 < p_{1,L}(\bar{L})$  corresponding to  $w_{\text{min}}(\bar{L}) < |w_{\text{st}}| < w_{\text{max}}$  with  $w_{\text{min}} \approx 0.07$  for  $\bar{L} = 20$ . The resulting curve is shown in Fig. 3(a,b) as violet solid line. A corresponding asymptotic estimate is shown in Fig. 3(a) as dashed line. There is also a shape  $\text{II}_1^*$  corresponding to local maximum, which plays the role of a possible transition state, for which we find the analogous result

$$E_{\text{tot},\text{II}_1^*} = \frac{1}{2}(E_{\text{tot},\text{II}_2^*} + E_{\text{tot},\text{II}_0}) \quad (88)$$

This maximum corresponds to a shape with a *small* bulge which is unstable with respect to shrinking to zero size to a shape  $\text{II}_0$  or to expanding to its equilibrium size in state  $\text{II}_1$ . The shape  $\text{II}_1^*$  exists for  $0 < p_1 < p_{\text{max}}$  corresponding to  $0 < |w_{\text{st}}| < w_{\text{max}}$  and is shown in Fig. 3(b) as violet dashed line.

**A.5 Other bulged shapes.** In principle, there exists also metastable states with bulges that extend to *both* sides of the groove on the same curved segment. Analogously to the results for shape  $\text{II}_2$ , we can calculate the length  $L_{\text{bul}}^*$  of such a bulge and the energy of a state  $\text{II}_4$  with two such bulges for fixed total adhered length  $L_{\text{st}} = L - 2L_{\text{bul}}^*$  from

$$2L_{\text{bul}}^* = L - L_{\text{st}} = \left(\frac{2\kappa}{\nu}\right)^{1/2} k_1(p) \quad (89)$$

$$k_1(p) \equiv \left(\int_0^\pi + 4\int_\pi^{\theta_{\text{inf}}}\right) d\theta (p + \sin\theta)^{-1/2} \quad (90)$$

$$a_{\text{st}} = 2\left(\frac{\kappa}{2\nu}\right)^{1/2} h_2(p)$$

$$k_2(p) \equiv -\left(\int_0^\pi + 4\int_\pi^{\theta_{\text{inf}}}\right) d\theta \cos\theta (p + \sin\theta)^{-1/2} \quad (91)$$

resulting in

$$\bar{L}_{\text{bul}}^* = \frac{k_1(p)}{k_2(p)} \quad (92)$$

$$\bar{L}_{\text{st}} = \bar{L} - \frac{2k_1(p)}{k_2(p)} \quad (93)$$

$$\frac{\nu a_{\text{st}}^2}{\kappa} = \frac{1}{2} k_2(p)^2 \quad (94)$$



and

$$E_b = 2E_{\text{bul}}^* = (2\kappa\nu)^{1/2}k_3(p)$$

$$\bar{E}_b = k_2(p)k_3(p)$$

$$k_3(p) \equiv \left( \int_0^\pi + \int_\pi^{\theta_{\text{int}}} \right) d\theta (p + \sin\theta)^{1/2} \quad (95)$$

This gives together with (93) a parametric representation of  $E_b(L_{st})$  using the parameter  $p$  in the range  $0 < p < p_{4,L}(\bar{L})$  of accessible parameters  $p$ , where  $p_{4,L}(\bar{L})$  is determined by the condition that  $\bar{L}_{st} < 0$  for  $p > p_{L,4}(\bar{L})$ .

The resulting parametric representation of  $E_b(L_{st})$  shows that  $E_{b,\text{II4}}(L_{st}) > E_{b,\text{II2}}(L_{st})$  for all possible values of  $L_{st}$ . Therefore, the bending energies of bulges which extend to both sides of the groove are always higher in bending energy for the same adhered length  $L_{st}$ .

## B Analytical energy minimization for ring condensation

In this appendix we derive exact analytical result for the metastable racquet shape of a ring in the presence of a polymer-polymer attraction  $W_{\text{con}} < 0$  per contact length.

The racquet shape consists of two round bulges, which assume the same length  $L_{\text{bul}}$  in equilibrium according to analogous arguments as for rings on the topographical stripe, and two adhering straight segments with total length  $L_{\text{con}}$ , which are in contact with contact energy  $-|W_{\text{con}}|L_{\text{con}}/2$ .

The ring closure constraint for the coordinate perpendicular to the adhering segments is

$$\int_{L_{\text{bul}}} ds \sin\theta(s) = 0 \quad (96)$$

which we associate with a Lagrange multiplier  $\nu$ . The Euler Lagrange equations and their first integral are identical to eqn (46) and (47) for the shape  $\text{II}_0$ , the integration constant  $c$  also defines a parameter  $p \equiv c/\nu$ .

The bulges of the racquet shape can be treated analogously to the bulges of shape  $\text{II}_4$  for the topographical surface groove, and we find

$$2L_{\text{bul}} = L - L_{\text{con}} = \left(\frac{2\kappa}{\nu}\right)^{1/2} k_1(p) \quad (97)$$

The ring closure constraint (96) gives

$$0 = \left(\frac{\kappa}{2\nu}\right)^{1/2} k_2(p) \quad (98)$$

such that  $p = p_0 \approx 0.46$  must be a zero of the elliptic function  $k_2(p)$  defined in (91). Eqn (97) with  $p = p_0$  then gives the Lagrange multiplier  $\nu$  as a function of the contact length  $L_{\text{con}}$ . The bending energy is

$$E_b = (2\kappa\nu)^{1/2}k_3(p_0) \quad (99)$$

as a function of  $\nu$ .

If the constraint of fixed contact length  $L_{\text{con}}$  is lifted the condition of contact curvature at the contact points gives  $c = |W_{\text{con}}|$  and, thus, determines the Lagrange multiplier  $\nu = |W_{\text{con}}|/p_0$ . Using this we obtain for the contact length from eqn (97),

$$\frac{L_{\text{con}}}{L} = 1 - \left(\frac{\kappa}{|W_{\text{con}}|L^2}\right)^{1/2} (2p_0)^{1/2}k_1(p_0) \quad (100)$$

and for the bending energy

$$\frac{E_b L}{\kappa} = \left(\frac{|W_{\text{con}}|L^2}{\kappa}\right)^{1/2} \frac{2^{1/2}k_3(p_0)}{p_0^{1/2}} \quad (101)$$

The total energy  $E_{\text{tot, rac}} = E_b - |W_{\text{con}}|L_{\text{con}}/2$  is obtained as

$$\frac{E_{\text{tot, rac}} L}{\kappa} = \left(\frac{|W_{\text{con}}|L^2}{\kappa}\right)^{1/2} (2p_0)^{1/2} \left(\frac{k_3(p_0)}{p_0} + \frac{k_1(p_0)}{2}\right) - \frac{1}{2} \frac{|W_{\text{con}}|L^2}{\kappa} \quad (102)$$

with  $(2p_0)^{1/2}(k_3(p_0)/p_0 + k_1(p_0)/2) \approx 12.85$ . This result holds for nonzero contact length  $L_{\text{con}} > 0$  or  $|W_{\text{con}}|L^2/\kappa > 2p_0k_1^2(p_0) \approx 73.33$ .

## 7 Acknowledgments

We acknowledge financial support by the Deutsche Forschungsgemeinschaft *via* Sonderforschungsbereich 448.

## References

- 1 S. Sheiko and M. Möller, *Chem. Rev.*, 2001, **101**, 4099–4123.
- 2 P. Samori, *J. Mater. Chem.*, 2004, **14**, 1353–1366.
- 3 A. Amzallag, C. Vaillant, M. Jacob, M. Unser, J. Bednar, J. Kahn, J. Dubochet, A. Stasiak and J. Maddocks, *Nucleic Acids Res.*, 2006, **34**, e125.
- 4 M. Sano, A. Kamino, J. Okamura and S. Shinkai, *Science*, 2001, **293**, 1299–1301.
- 5 J. Tang, J. Käs, J. Shah and P. Janmey, *Eur. Biophys. J.*, 2001, **30**, 477–484.
- 6 D. Hatters, C. MacRaild, R. Daniels, W. Gosal, N. Thomson, J. Jones, J. Davis, C. MacPhee, C. Dobson and G. Howlett, *Biophys. J.*, 2003, **85**, 3979–3990.
- 7 K. Alim and E. Frey, *Phys. Rev. Lett.*, 2007, **99**, 198102.
- 8 G. Linke, R. Lipowsky and T. Gruhn, *Phys. Rev. E: Stat., Nonlinear, Soft Matter Phys.*, 2005, **71**, 051602.
- 9 N. Severin, W. Zhuang, C. Ecker, A. Kalachev, I. Sokolov and J. Rabe, *Nano Lett.*, 2006, **6**, 2561–2566.
- 10 M. Hochrein, J. Leierseder, L. Golubović and J. O. Rädler, *Phys. Rev. Lett.*, 2006, **96**, 038103.
- 11 M. Hochrein, J. Leierseder, L. Golubović and J. O. Rädler, *Phys. Rev. E: Stat., Nonlinear, Soft Matter Phys.*, 2007, **75**, 021901.
- 12 V. Bloomfield, *Biopolymers*, 1991, **31**, 1471–1481.
- 13 V. Bloomfield, *Biopolymers*, 1997, **44**, 269–282.
- 14 B. Schnurr, F. MacKintosh and D. Williams, *Europhys. Lett.*, 2000, **51**, 279–285.
- 15 B. Schnurr, F. MacKintosh and D. Williams, *Phys. Rev. E: Stat., Nonlinear, Soft Matter Phys.*, 2002, **65**, 061904.
- 16 Čebers, Z. Dogic and P. A. Janmey, *Phys. Rev. Lett.*, 2006, **96**, 247801.
- 17 O. Pierre-Louis, *Phys. Rev. E: Stat., Nonlinear, Soft Matter Phys.*, 2008, **78**, 021603.
- 18 K. Brakke, *Exp. Math.*, 1992, **1**, 141–165.
- 19 U. Seifert and R. Lipowsky, *Phys. Rev. A: At., Mol., Opt. Phys.*, 1990, **42**, 4768–4771.
- 20 U. Seifert, *Phys. Rev. A: At., Mol., Opt. Phys.*, 1991, **43**, 6803–6814.
- 21 J. Kierfeld and R. Lipowsky, *Europhys. Lett.*, 2003, **62**, 285–291.
- 22 J. Kierfeld, *Phys. Rev. Lett.*, 2006, **97**, 058302.
- 23 P. Kraikivski, R. Lipowsky and J. Kierfeld, *Europhys. Lett.*, 2004, **66**, 763–769.
- 24 P. Kraikivski, R. Lipowsky and J. Kierfeld, *Eur. Phys. J. E*, 2005, **16**, 319–340.